GEORGIA DOT RESEARCH PROJECT 20-18

Final Report

RECOMMENDATIONS FOR EXTENSION IN SERVICE LIFE OF ASR-AFFECTED CONCRETE

Georgia Department of Transportation

Office of Performance-based Management and Research
600 West Peachtree Street NW | Atlanta, GA 30308

August 2024

TECHNICAL REPORT DOCUMENTATION PAGE

1. Report No.: FHWA-GA-24-2018	2. Government Accession No.: N/A	3. Recipient's Catalog No.: N/A
4. Title and Subtitle: Recommendations for Extension in Service Life of ASR-Affected Concrete		5. Report Date: August 2024
		6. Performing Organization Code: N/A
7. Author(s): Kimberly E. Kurtis (PI), Ph.D., Lauren K. Stewart (PI), Ph.D., Devin Kumar (Graduate Research Assistant)		8. Performing Organization Report No.: 20-18
9. Performing Organization Name and Address: Georgia Institute of Technology 790 Atlantic Drive Atlanta, GA 30332		10. Work Unit No.: N/A
		11. Contract or Grant No.: PI#0017433
12. Sponsoring Agency Name and Address: Georgia Department of Transportation (SPR) Office of Performance-based Management and Research 600 West Peachtree St. NW Atlanta, GA 30308		13. Type of Report and Period Covered: Final Report (August 2020–August 2024)
		14. Sponsoring Agency Code: N/A
15. Supplementary Notes: Prepared in cooperation with the U.S. Department of Transportation, Federal Highway Administration.		

16. Abstract:

Alkali–silica reaction (ASR), a chemical reaction occurring in concrete between reactive siliceous minerals in some aggregates and alkalis in the concrete pore solution, can produce an expansive gel that, in the presence of sufficient moisture, can lead to expansion and cracking. This not only decreases mechanical properties but also increases permeability and, as a result, increases potential for degradation by other aggressive agents. Common methods to mitigate damage or repair of affected concrete include surface coatings and external confinement. New approaches that claim to better extend the service life of ASR-affected concrete are being used in the field but have not yet been systematically evaluated. In this report, laboratory-cast concrete and field concrete—both affected by ASR—were repaired to examine the performance of a range of existing and emerging repair materials. Laboratory-cast samples were repaired with silane- and nanosilica-based coatings, and others were confined with fiber-reinforced ultra-high performance concrete (UHPC). In the field, cracked concrete traffic (i.e., Jersey) barriers were repaired with flexible caulk and surface-treated with silanes and slurries. The efficacy of each is being monitored through measurements of expansion and crack growth. Recommendations for repair of ASR-affected transportation infrastructure are made, depending on the initial level of ASR-damage. These recommendations begin with silanes for mild to moderate conditions and increase in repair potential to the most rigorous recommendations of structural confinement.

17. Keywords: Alkali-silica reaction, concrete, durability, repair		18. Distribution Statement: No Restriction	
19. Security Classification: Unclassified	20. Security Classification (of this page): Unclassified	21. No. of Pages: 74	22. Price: Free

Form DOT 1700.7 (8-72) Reproduction of completed page authorized

GDOT Research Project 20-18

Final Report

RECOMMENDATIONS FOR EXTENSION IN SERVICE LIFE OF ASR-AFFECTED CONCRETE

By

Dr. Kimberly E. Kurtis
Professor

Dr. Lauren K. Stewart
Associate Professor

Devin Kumar
Graduate Research Assistant

Georgia Tech Research Corporation

Contract with
Georgia Department of Transportation

In cooperation with
U.S. Department of Transportation, Federal Highway Administration

August 2024

SI* (MODERN METRIC) CONVERSION FACTORS

APPROXIMATE CONVERSIONS TO SI UNITS

Symbol	When You Know	Multiply By	To Find	Symbol
		LENGTH		
in	inches	25.4	millimeters	mm
ft	feet	0.305	meters	m
yd	yards	0.914	meters	m
mi	miles	1.61	kilometers	km
		AREA		
in^2	square inches	645.2	square millimeters	mm^2
ft^2	square feet	0.093	square meters	m^2
yd^2	square yard	0.836	square meters	m^2
ac	acres	0.405	hectares	ha
mi^2	square miles	2.59	square kilometers	km^2
		VOLUME		
fl oz	fluid ounces	29.57	milliliters	mL
gal	gallons	3.785	liters	L
ft^3	cubic feet	0.028	cubic meters	m^3
yd^3	cubic yards	0.765	cubic meters	m^3
		NOTE: volumes greater than 1000 L shall be shown in m^3		
		MASS		
oz	ounces	28.35	grams	g
lb	pounds	0.454	kilograms	kg
T	short tons (2000 lb)	0.907	megagrams (or "metric ton")	Mg (or "t")
		TEMPERATURE (exact degrees)		
^oF	Fahrenheit	5 (F-32)/9 or (F-32)/1.8	Celsius	^oC
		ILLUMINATION		
fc	foot-candles	10.76	lux	lx
fl	foot-Lamberts	3.426	candela/m^2	cd/m^2
		FORCE and PRESSURE or STRESS		
lbf	poundforce	4.45	newtons	N
lbf/in^2	poundforce per square inch	6.89	kilopascals	kPa

APPROXIMATE CONVERSIONS FROM SI UNITS

Symbol	When You Know	Multiply By	To Find	Symbol
		LENGTH		
mm	millimeters	0.039	inches	in
m	meters	3.28	feet	ft
m	meters	1.09	yards	yd
km	kilometers	0.621	miles	mi
		AREA		
mm^2	square millimeters	0.0016	square inches	in^2
m^2	square meters	10.764	square feet	ft^2
m^2	square meters	1.195	square yards	yd^2
ha	hectares	2.47	acres	ac
km^2	square kilometers	0.386	square miles	mi^2
		VOLUME		
mL	milliliters	0.034	fluid ounces	fl oz
L	liters	0.264	gallons	gal
m^3	cubic meters	35.314	cubic feet	ft^3
m^3	cubic meters	1.307	cubic yards	yd^3
		MASS		
g	grams	0.035	ounces	oz
kg	kilograms	2.202	pounds	lb
Mg (or "t")	megagrams (or "metric ton")	1.103	short tons (2000 lb)	T
		TEMPERATURE (exact degrees)		
^oC	Celsius	1.8C+32	Fahrenheit	^oF
		ILLUMINATION		
lx	lux	0.0929	foot-candles	fc
cd/m^2	candela/m^2	0.2919	foot-Lamberts	fl
		FORCE and PRESSURE or STRESS		
N	newtons	0.225	poundforce	lbf
kPa	kilopascals	0.145	poundforce per square inch	lbf/in^2

* SI is the symbol for the International System of Units. Appropriate rounding should be made to comply with Section 4 of ASTM E380. (Revised March 2003)

TABLE OF CONTENTS

LIST OF FIGURES

LIST OF TABLES

CHAPTER 1. INTRODUCTION

MOTIVATION

Cracking, staining, and spalling on concrete infrastructure resulting from alkali–silica reaction (ASR) is increasingly common, including in Georgia, with ASR damage noted in roadways, airfields, dams, retaining walls, and bridges around the state (e.g., figure 1). ASR can reduce stiffness and strength. Interconnected cracking can compromise concrete permeability, allowing for other aggressive agents to enter the concrete. In some cases, structural concrete or concrete pavements are so compromised by ASR that they require extensive repair or outright replacement.

Figure 1. Illustration. ASR-affected bridge support in Atlanta, Georgia.

The mineralogical characteristics of aggregates available to Georgia concrete producers include metamorphized granites and sands containing cherty and other potentially alkali-reactive components. The damaging effects of the use of these materials alone or in combination is becoming evident as infrastructure ages, even more so without ASR mitigation implemented in the mixture design. As nonreactive aggregate sources, particularly in metropolitan areas, are becoming depleted, new sources and existing marginal aggregate sources have begun to be exploited. That is, the ASR issues affecting the state's concrete infrastructure are only expected to increase. Thus, guidance is needed for: (1) assessing the condition state in potentially ASR-affected concrete, (2) determining the potential for further reaction and damage, and (3) identifying both the material and/or structural means to extend the service life of ASR-affected concrete until significant repair and/or reconstruction can be undertaken.

Several approaches have been explored for extending the service life of ASR-affected concrete. These range from surface-applied chemicals and waterproofing and flexible coatings to external strengthening. Lithium admixtures have been known for decades to reduce ASR expansion, as measured in laboratory testing, by affecting the structure and swelling capacity of the ASR gel product. However, field studies have not shown benefits of lithium when applied to concrete surfaces or when penetrated into concrete through an electrochemical process [1], [2]. Because costs for lithium have increased substantially in recent years due to the high demand for this material in batteries, further exploration of lithium admixtures for mitigation of ASR expansion does not seem to be promising [3].

A more effective strategy is minimizing the availability of water and thus limiting the potential for further reaction and gel expansion. For many reactive aggregates, ASR slows significantly at internal relative humidity (RH) of less than 80–85 percent. However, this limit needs to be validated for reactive aggregates in Georgia because the limit depends on the nature of the reactive siliceous mineral(s) present [4]. Reductions in internal humidity can be accomplished through a combination of water control on-site, crack filling, and the application of surface coatings that resist water penetration. Breathable sealers such as silanes have been shown to mitigate ASR expansion in existing structures [5] and pavements [6], [7]. However, others have found silanes to be ineffective because of low penetration depths and low resistance to environmental degradation [8], which emphasizes the inherent difficulty in mitigation. Most recently, silane coatings containing colloidal nanosilica have been proposed to treat salt-damaged concrete, but their effect on ASR-affected concrete has not been well-documented in the literature [9]. Because of the variation in effectiveness among coatings and the importance of substrate preparation and environmental conditions, testing or compilation of a database of past test results is needed to identify the most promising solutions.

Waterproof membranes and overlays also have been investigated for slowing ASR damage [8]. These range from elastomeric polymers to cement-based composites to asphalt overlays. Although some studies have shown that they are ineffective in suppressing further ASR expansion, such measures can address aesthetic effects of ASR. More recent studies suggest a combination of silanes and membranes can be quite effective, particularly when combined with crack filling [10]. Crack filling with epoxy or flexible caulking are the most common practices.

Structural techniques, such as the addition of external reinforcement with steel or fiber-reinforced polymer jacketing or layering, has also been attempted to restrain expansion and physically strengthen the element [11], [12]. Plate bonding technology [8] and post-tensioning with steel rods or cables are additional mechanical techniques that can be used to strengthen or restrain ASR-affected structures. Post-tensioning can be a useful approach where there is a need to limit expansion due to compatibility issues, and this technique is particularly needed in structures regularly exposed to or immersed in water where environmental control measures would be impractical. These approaches have been primarily used in large structural elements, such as those in bridge substructures [13]. Past studies have also indicated that promising material-based approaches may create structural issues, such as the yielding of steel reinforcement at bends, which must be properly detailed to account for such repair methods [14].

This research seeks to examine both new and existing repair techniques, including combinations of surface treatment and structural repair, and identify the most promising strategies.[1] The selection of repair strategies was informed through the results of a 2020 survey, performed with the Georgia Department of Transportation's (GDOT) support, of the American Association of State Highway and Transportation Officials (AASHTO) Subcommittee on Materials (SOM) members and through consultation with ASR-repair consultants, researchers, and materials providers. Of the 50 states surveyed, 11 responded. Among those, 73 percent indicated that their state had experienced ASR damage to its transportation infrastructure (figure 2). However, most respondents did not provide details on repair strategies, suggesting that research such as that performed in this study is necessary to provide further basis for identification of effective ASR repair methods.

[1] Use of waterproof membranes for repair were not included in this investigation, although crack-filling was employed.

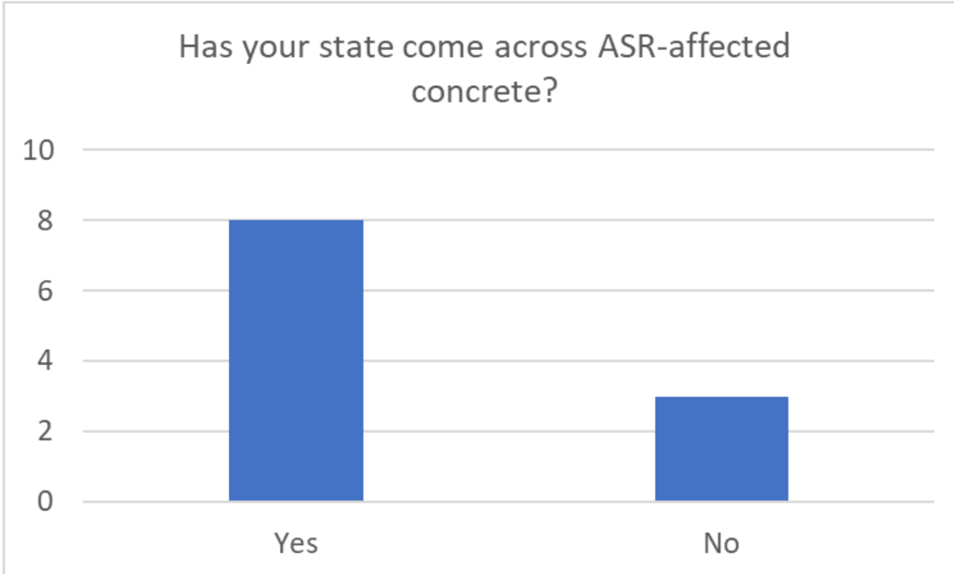

Figure 2. Graph. AASHTO SOM survey results:
Has your state come across ASR-affected concrete?

It is critical that evaluation be performed at-scale. For example, studies at The University of Texas at Austin have established that coatings that work well for small-scale laboratory specimens do not necessarily perform as well in the field [15], [16] because of the greater difficulty in reducing RH within a larger volume of concrete. Conducted at Georgia Institute of Technology's (Georgia Tech) Structural Engineering and Materials Laboratory (SEML), this research explores both surface coatings and external confinement for repair of large-scale ASR-affected concrete elements. Reinforced and unreinforced ASR-affected concrete cast for this research and obtained from the field are studied before and after repair.

RESEARCH OBJECTIVES

The objectives of this research are as follows:

1. To provide a review of current technology and "best practices" for extending the service life of ASR-affected concrete.
2. To develop approaches for assessing the condition state in potentially ASR-affected concrete and determine the potential for further reaction and damage.
3. To develop combined coating and confinement repair strategies to extend the service life of ASR-affected concrete.

REPORT ORGANIZATION

Chapter 2 details the design, construction, monitoring, and repair of large-scale laboratory concrete columns and slabs in this project. Materials selection, mixture design, and design criteria are provided, followed by descriptions of the accelerating conditions used to support the occurrence of ASR damage during the investigation period. Following the appearance of visible surface-breaking cracking, repair was initiated, and this chapter describes those approaches as well as the ongoing monitoring. Repairs examined in this chapter include confinement and surface coatings.

Chapter 3 describes the characterization, monitoring, and repair of field ASR-affected concrete traffic (i.e., Jersey) barriers obtained from the field. This chapter focuses on the assessment of seven different surface-coating repair materials.

Chapter 4 summarizes the outcomes to date and makes recommendations for repair of ASR-affected concrete. Additionally, future needs for research, including early detection of ASR-affected concrete and improvements in characterization, are identified.

CHAPTER 2. REPAIR AND MONITORING OF LARGE-SCALE LABORATORY-CAST CONCRETE

INTRODUCTION

Large-scale concrete elements were cast with reactive aggregate and with increased alkali content in concrete. These were designed to experience ASR damage during the duration of the research program, followed by repair. Monitoring of expansion and damage started after casting and continues.

Laboratory-cast samples have some advantages over field samples. These advantages include control over sample geometry and design, as well as control of the material constituent's mixture design. A priority was to select materials and mixture proportions that would reflect GDOT practices and create samples that may realistically be found in Georgia. As a result, aggregates were selected from GDOT's Qualified Product List (QPL), with accelerated testing performed to identify a potentially reactive aggregate from a regional source. All materials were locally sourced. Concrete columns and slab samples were designed using GDOT specifications, and rectangular columns, circular columns, bridge deck samples (reinforced slabs), and pavements (unreinforced slabs) were produced.

Samples were placed in an accelerating environment until external cracking, which is typically the first visually recognizable sign of ASR-damage, was evident. Samples were then repaired using three commercially available surface coatings or external confinement. This chapter details the sample design, construction, and monitoring before and after repair.

MATERIALS AND TEST METHODS

Cement

For all concrete and mortar mixtures, an ASTM C150 Type I/II cement (Heidelberg Materials, formerly Lehigh Cement Company in Leeds, Alabama) was used. The physical characteristics are given in table 1, and the cement composition is given in table 2. The cement equivalent alkali content (Na_2O_{eq}) is 0.52 percent by mass, as reported by the producer.

Table 1. Physical characteristics of cement from mill report.

Physical Characteristic	Value
Na_2O_{eq} Eqv (%)	0.52
Heat of hydration (k/kg) 3 days	314
Loss on ignition (LOI)	2.51
Fineness (% passing through 45 µm)	96
Fineness (Blaine fineness, m^2/kg)	406
Air content (%)	6
Density (g/cm^3)	3.14

Table 2. Composition of cement from mill report.

Classification	Chemical Composition	%
Oxide	SiO_2	10.60
	Al_2O_3	4.35
	Fe_2O_3	2.3
	CaO	49.75
	SO_3	0.41
Phase	C_3S	53.88
	C_2S	19.46
	C_3A	7.13
	C_4AF	9.17

Aggregate Sourcing and Testing

The first step in sourcing local materials was to find a reactive aggregate capable of generating ASR damage within the laboratory-cast concrete during the project period of performance. It was also important to choose a moderately reactive aggregate to better reflect field conditions; that is, aggregate testing for ASR is part of the qualification of a material source by GDOT, so highly reactive aggregate would not be used in state construction. Various coarse [17] and fine aggregates [18] from GDOT's QPL were initially tested by accelerated mortar bar testing (AMBT), ASTM C1260 [19] (Standard Test Method for Potential Alkali Reactivity of Aggregates), which soaks mortar bars composed of the tested aggregate in a 1 N NaOH solution at 80°C.

Based on these results, a fine aggregate (a concrete sand from Wiregrass Construction in Gadsen, Alabama) was chosen. The 14-day expansion averaged 0.14 percent, which places it above the 0.1 percent limit for likely innocuous behavior and below the potentially deleterious lower bound of 0.2 percent expansion [19]. Additionally, a non-reactive coarse aggregate (67-stone from Vulcan Materials in Forest Park, Georgia) was used in the concrete production. The 14-day expansion averaged 0.02 percent for this aggregate in the AMBT, as shown in figure 3 along with the lower 0.1 percent limit (dashed horizontal gray line) and the 0.2 percent limit (dashed horizontal red line). Table 3 presents other relevant properties of these aggregates, such as maximum aggregate size (MSA), bulk specific gravity (BSG), dry rodded unit weight (DRUW), fineness modulus (FM), and percent absorption.

Table 3. Relevant properties of aggregates.

Properties	Coarse Aggregate	Fine Aggregate
MSA	0.75 inch	N/A
BSG	2.655	2.588
DRUW	103 lb/ft^3	N/A
FM	N/A	2.75
% absorption	0.62	1

N/A = not applicable.

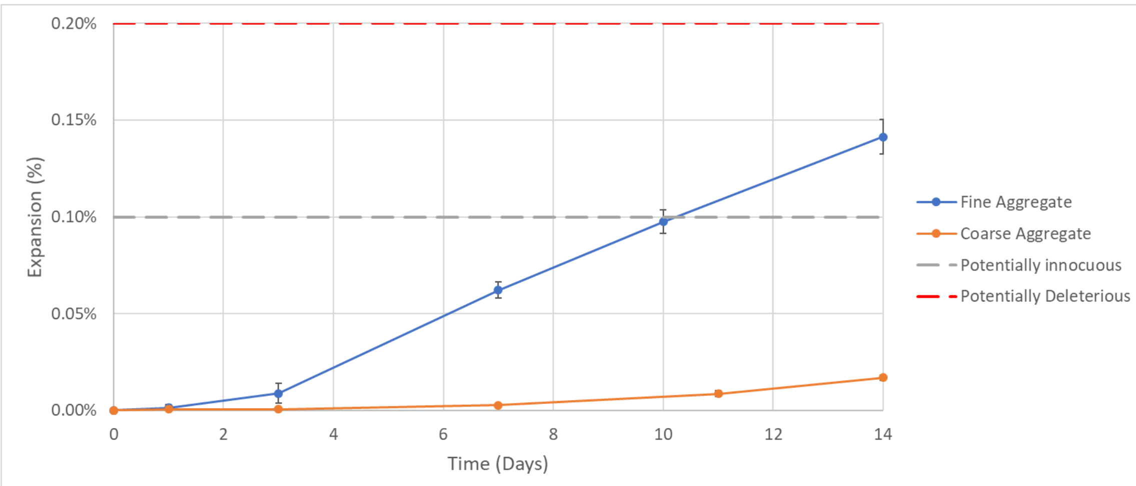

Figure 3. Graph. ASTM C1260 results for fine and coarse aggregates.

After testing, cut mortar bar cross sections were examined under a light microscope (Leica MZ6), using methods in ASTM C856-14 [20] (Standard Practice for Petrographic Examination of Hardened Concrete) Appendix X1. Bars were cut using a slow-speed rotating saw (Allied TechCut 4) with ethanol as a lubricant and then were stained with uranyl acetate solution, $UO_2(C_2H_3O_2)_{2.2}H_2O$. The sample was illuminated with ultraviolet (UV) light (λ = 254 nm) at 16× magnification. Figure 4 shows a cross section of the mortar bar produced with the fine aggregate under (a) white light and (b) UV light, along with the coarse aggregate under (c) white light and (b) UV light at the same magnification. Fluorescence within the cracks of the fine aggregate and at the rims indicates ASR gel and confirms the potential for reactivity with this source. Contrary, a lack of fluorescence or the presence of cracking within the microstructure indicates a lack of reactivity for the coarse aggregate.

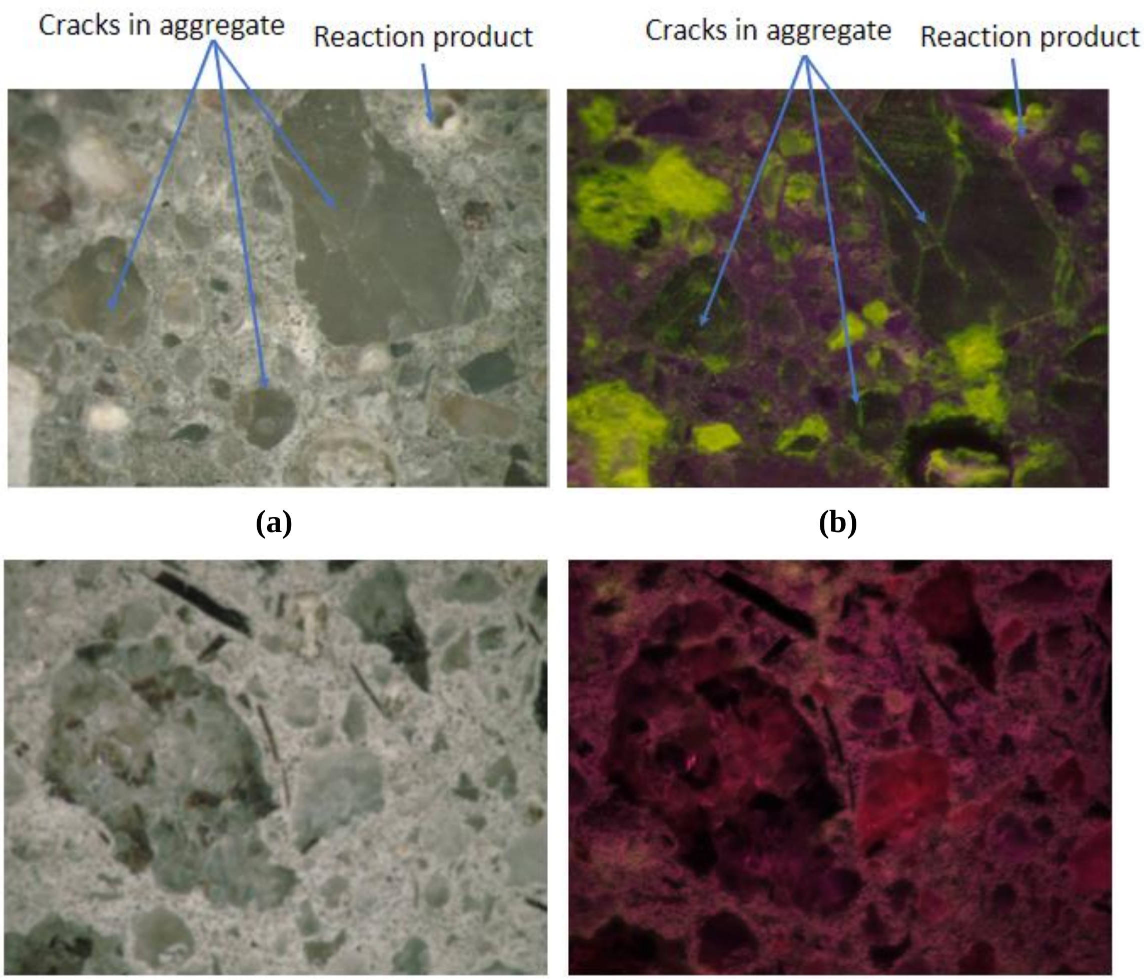

(a) (b)

(c) (d)

Figure 4. Illustration. Uranyl acetate–stained petrography of reactive fine aggregate under (a) white light and (b) UV light and non-reactive coarse aggregate under (c) white light and (d) UV light at 16x magnification

Further, both fine and coarse aggregates were subjected to the Federal Highway Administration (FHWA) T-FAST (Turner-Fairbank Highway Research Center ASR Susceptibility Test) [21]. The T-FAST is a 21-day test performed by (1) subjecting powdered aggregates to a strongly alkaline solution at high temperature to dissolve mineral phases and, subsequently, (2) measuring electrical conductivity of the solution produced, as well as concentrations of aluminum, calcium, and silicon, to assess reactivity levels of the aggregate. Four different conditions, which vary in their CaO content and temperature (55°C or 80°C), are used to assess aggregate reactivity. The test classifies the aggregate reactivity (i.e., slow, moderate, or high) and also can predict a maximum threshold of alkalis in the concrete before ASR initiates. T-FAST results for both aggregates, including the reactivity classifications based on condition scores (1–4) and alkali thresholds, are provided in table 4. Validating the AMBT results, the fine aggregate was classified as between moderately and highly reactive. The coarse aggregate was classified as slowly reactive, although it was noted by FHWA as unlikely to independently undergo ASR distress in the field based on the high alkali threshold value. The combined alkali threshold of both aggregates, at the proportions used in the laboratory cast samples (see Structural design of concrete), was 3.37 lb/yd^3. This value was used in the design of the concrete mixtures to ensure reactivity.

Table 4. T-FAST results of fine and coarse aggregate.

Aggregate	Condition				Reactivity Classification	Alkali Threshold (lb/yd^3)
	1	2	3	4		
Fine	10.88	16.03	15.02	107.1	Moderately/highly reactive	3.71
Coarse	0.99	0.44	0.33	6.15	Slowly reactive	>10.96

Concrete Prism Testing

Additionally, concrete prisms (3 inch × 3 inch × 10 inch) were cast and subjected to ASTM C1293 [22] (Standard Test Method for Determination of Length Change of

Concrete Due to Alkali–Silica Reaction) conditions, including an average temperature of 100°F (38°C) and being held over water in sealed containers. Expansions were monitored for one year (August 2022 – August 2023). Rather than using the standard's specified mixture design [22], prisms were cast from each casting of the large-scale samples. In this way, these test results provide a basis of (1) reactivity of the concrete mixture design, (2) measurement of consistency between concrete batches, and (3) accelerated indication of potential expansions. Average prism expansions from all batches of casting are provided in figure 5; the 52-week average expansion is 0.26 percent. The variation among batches is at most 15.8 percent (from the overall average) and 29.5 percent (from the lowest to the highest overall average), which is consistent with the standard of no more than 40 percent variation of the average test result for more than 0.02 percent average expansion.

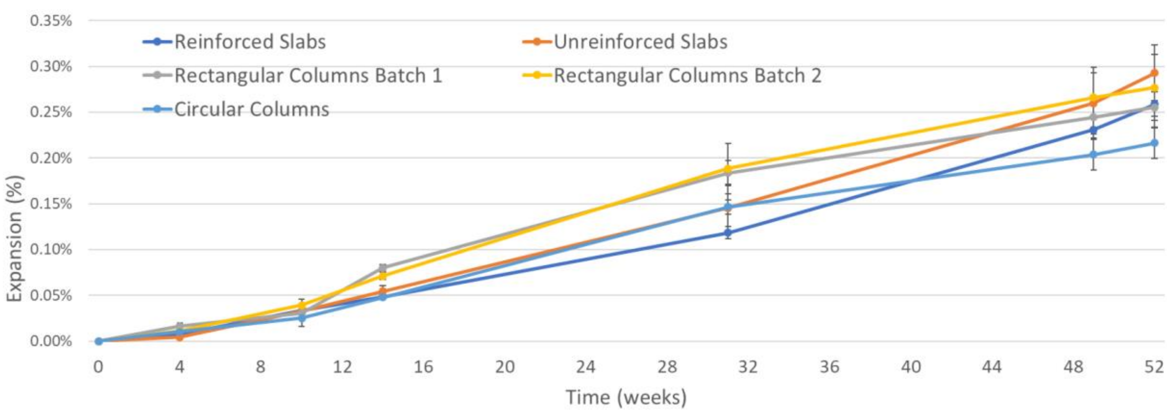

Figure 5. Graph. One-year expansion data for prisms cast from concrete mixture design used to produce structural elements (see table 3).

Mixture Design

GDOT's concrete mix design specifications (Section 500) [23] were used as guidelines for design of the columns and slabs. The same mixture design (see table 5) was used for both elements, following guidance for Class AA as structural concrete. To accelerate ASR damage in the concrete, the alkali content was boosted to 1.25 percent Na_2O_{eq} by mass. This is the value prescribed in ASTM C1293, and this concentration was also used in prior research efforts on ASR repair so that meaningful expansion could occur at a reasonable time for repair to ensue [24], [25], [26] . With a cement alkali content of 0.52 percent, the remaining 0.73 percent was supplemented through the addition of sodium hydroxide with a conversion factor of 1.291 from NaOH to Na_2O_{eq} by mass.

The resulting total Na_2O_{eq} of the mixture design was 9.75 lb/yd^3, which was above the T-FAST alkali threshold of 3.37 lb/yd^3 for these aggregates in these proportions. This design suggests ASR can be induced readily in the cast samples, despite the moderate reactivity of the aggregate.

The overall mixture design is shown in table 5. Sodium hydroxide was provided in the form of a 50 percent by weight solution (Fisher Scientific). To account for the water in the alkali solution, the 7.35 lb/yd^3 reported is the amount of NaOH, with the remaining 50 percent of the solution accounted for in the water content. A retarding admixture (MasterSet DELVO, Master Builder Solutions) was added at a rate of 1 fl oz per 75 lb of cement to offset the acceleratory effect of the NaOH addition [27].

Table 5. Mixture design of laboratory-cast samples.

Material	Mass (lb/yd^3)
Water	345
Cement	780
Coarse aggregate	1655
Fine aggregate	1127
Retarding admixture	0.74
NaOH	7.35

STRUCTURAL DESIGN OF CONCRETE

Structural elements most commonly affected by ASR in the field were chosen for casting and for eventual repairs. These include reinforced circular and rectangular columns and reinforced and unreinforced slabs. For slabs, the unreinforced samples represent rigid pavements, and the reinforced samples represent bridge decks. GDOT design guides and existing typical structural drawings were used to inform the sample designs.

For the columns, Mander's Confinement Model [28]—a model that calculates confining pressure of concrete from reinforcement layouts that includes parameters such as reinforcement size, spacing, and overall geometry—was used as a basis for the reinforcement steel design. Because reinforcement in concrete is known to aid in preventing ASR expansion to a degree [29], [30], confinement provided by laboratory-cast samples needed to be comparable to full-scale structures. Table 6 outlines the reinforcement steel design and corresponding effective lateral pressure, f'_l, for the full-scale structure and respective sample for the circular and rectangular geometries. Both rectangular and circular samples were designed to be 2 ft wide and 4 ft 2 inches tall. Aside from typical stress concentrations presented at rectangular corners, circular columns are typically designed in seismic regions; thus, f'_l is appropriately higher than for the rectangular columns.

Table 6. Reinforcement design and effective lateral pressure.

Cross Section	Reinforcing Steel		f'_l (ksi)
	Longitudinal, Size (quantity)	Transverse, Size (spacing)	
3.5 ft Full-Scale Rect.	#11 (20)	#4 (12 inch O.C.)	0.0363
2 ft Sample Rect.	#9 (8)	#3 (9.6 inch O.C.)	0.0321
3 ft Full-Scale Circ.	#11 (8)	#4 (12 inch O.C.)	0.0431
2 ft Sample Circ.	#9 (8)	#3 (9.6 inch O.C.)	0.0417

O.C. = on center.

Design drawings of the circular and rectangular columns are shown in figure 6 and figure 7, respectively. In total, four rectangular samples and three circular samples were cast. One each of the rectangular and circular samples were unreinforced to compare the effects of reinforcement on the samples.

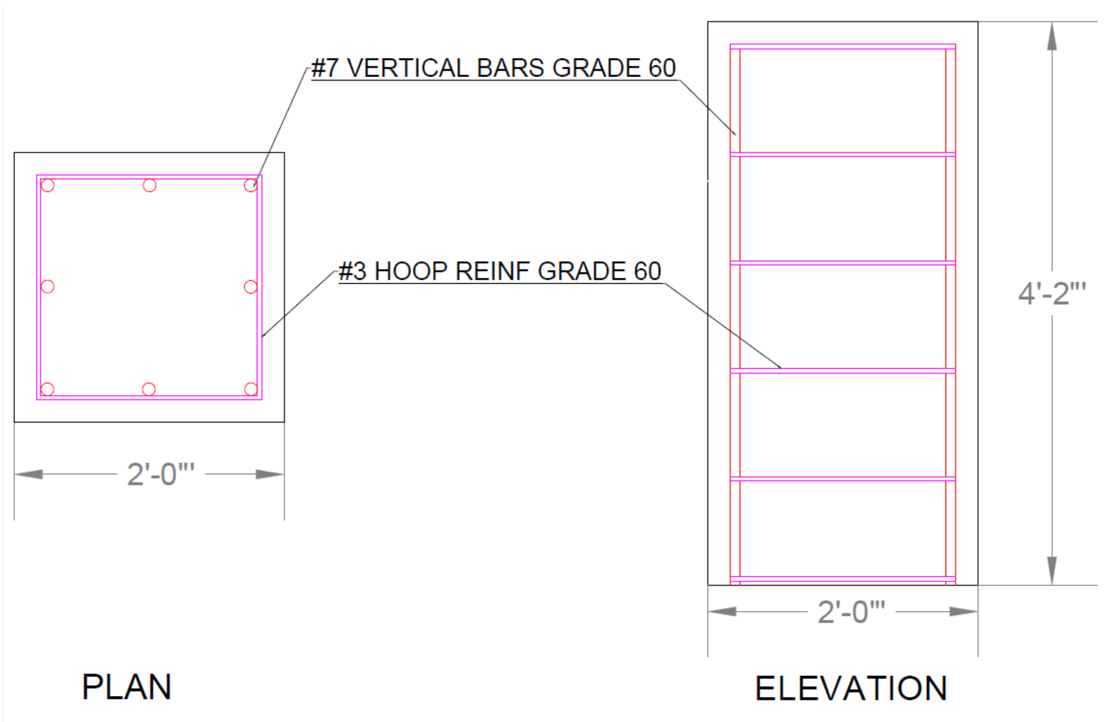

(a) **(b)**

Figure 6. Illustration. Design drawing of reinforced rectangular column samples in (a) plan view and (b) elevation view.

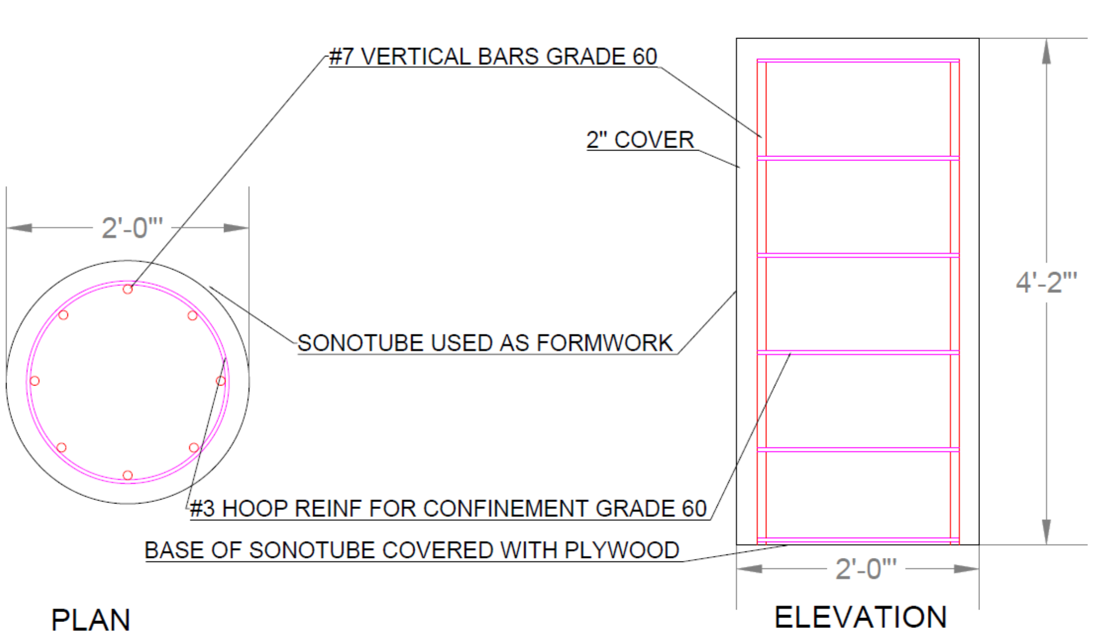

(a) **(b)**

Figure 7. Illustration. Design drawing of reinforced circular column samples in (a) plan view and (b) elevation view.

For the slabs, geometry and reinforcement were replicated to match a common GDOT design. Design drawings for the bridge decks are shown in figure 8. Bridge deck samples were designed to have reinforcement in both directions, and pavement samples matched the geometry of the bridge decks without reinforcement. Three bridge deck samples and three pavement samples were cast.

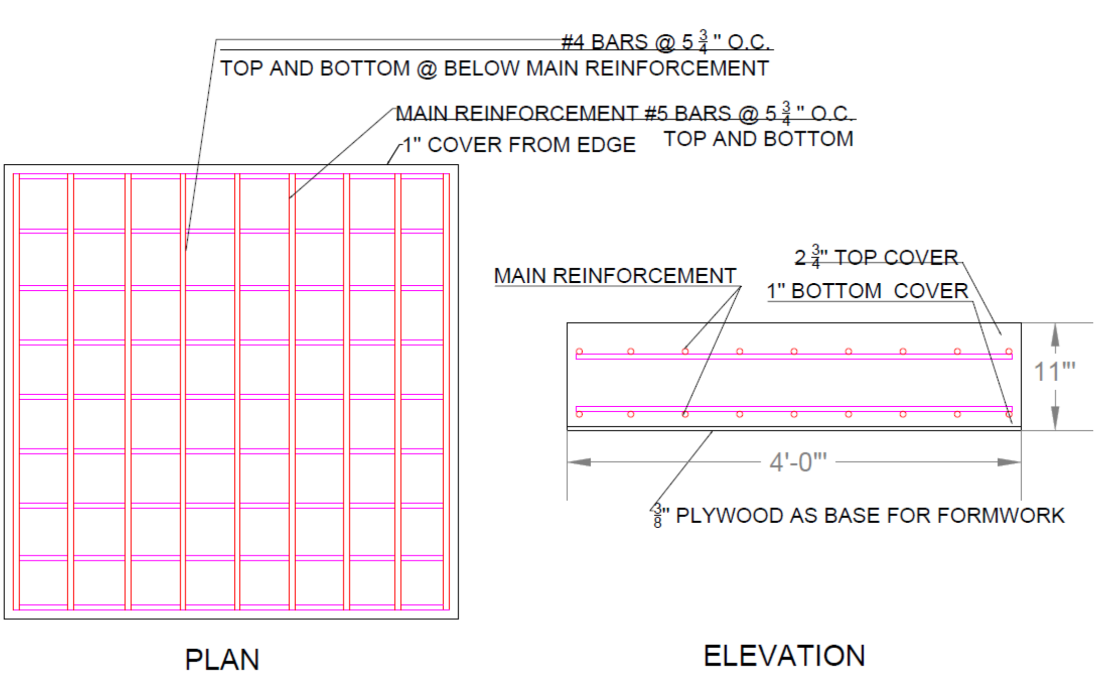

(a) **(b)**

Figure 8. Illustration. Design drawing of reinforced slab samples in (a) plan view and (b) elevation view.

To monitor deformations, instrumentation was cast within the samples. Embedded vibrating wire strain gauges (4200-06, Geokon) were installed in all specimens to monitor internal deformation. Their reported accuracy is 1 microstrain (με), and their reported range is 5000 με. In addition, insert studs were preplaced into the formwork to measure external deformation, using a multilength strain gauge set and large caliper for longer distances. The accuracies of the strain gauge set and caliper are 0.0002 and 0.002

inches, respectively. Finally, steel strain gauge sensors were attached to the rebar in the reinforced samples. Figure 9 shows the installation of the vibrating wire strain gauges. To maintain the sensors' orientation during placement, they were attached to small PVC pipes connected by twisted wire to the rebar.

Figure 9. Illustration. Installation of vibrating wire strain gauges.

CASTING OF SAMPLES

Samples were batched, mixed, and cast at Georgia Tech's SEML using a portable skid mixer (Skid Mount Portable Concrete Mixer, Cart Away) with 1.75 yd^3 batch capacity. The formwork is shown in figure 10. Materials were preweighed using a station setup, loaded by assembly, and placed using a forklift with a skid-mount attachment. Samples were cast from concrete batches as follows: (1) one 1.7 yd^3 batch for reinforced slabs (three samples) and one 1.7 yd^3 batch for unreinforced slabs (three samples), (2) two 1.3

yd^3 batches for rectangular columns (two samples each), and (3) one 1.6 yd^3 batch for circular columns (three samples). Vibration was performed using a handheld electric vibrator during pours. The casting process is shown in figure 11, figure 12, and figure 13.

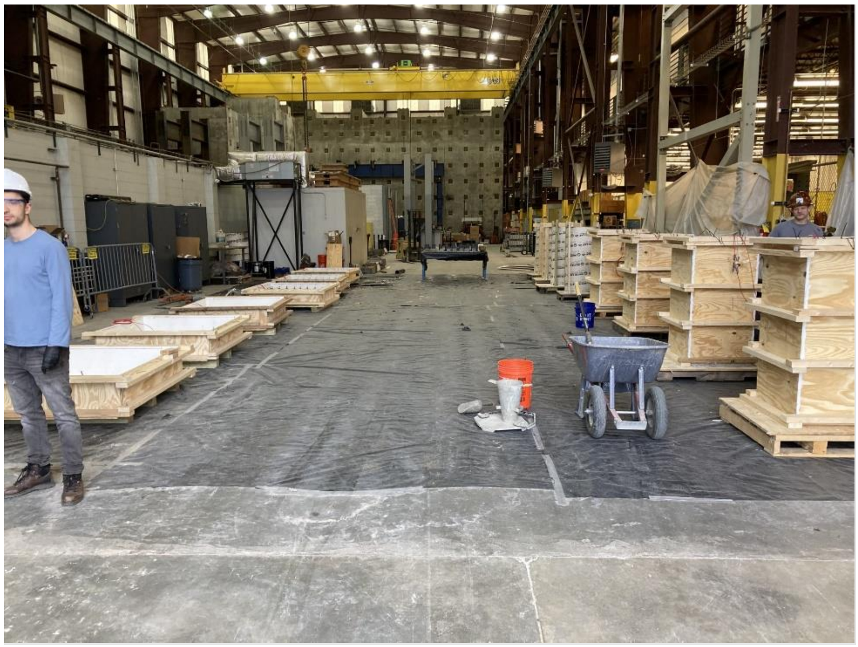

Figure 10. Illustration. Formwork of all samples laid out.

Figure 11. Illustration. Preweighing station of materials.

Figure 12. Illustration. Loading of materials into mixer.

Figure 13. Illustration. Dispensing of concrete into formwork using attached chute.

STORAGE OF SAMPLES

After casting, the samples' surfaces were covered in plastic sheeting. After 7 days, samples were moved to an environmental chamber, shown in figure 14(a), where they were maintained at 99 percent RH and 32° ± 8°C. Temperature and humidity control were provided by an industrial-grade humidifier (Ultrasonic Humidifier Atomizer) and blow heater (DXH1000TS, DeWalt), respectively, outlined in the schematic in figure 14(b). This environmental condition was chosen to accelerate ASR damage, allowing repairs to begin within the project timeframe. Sample nomenclature is included in table 7.

Table 7. Nomenclature for samples.

Acronym	Sample Name	Sample Numbers
RS	Reinforced Slab	1, 2, 3
US	Unreinforced Slab	1, 2, 3
CC	Circular Column	1, 2
UCC	Unreinforced Circular Column	3
RC	Reinforced Rectangular Column	1, 2, 3
URC	Unreinforced Rectangular Column	4

(a) **(b)**

Figure 14. Illustration. Samples in environment chamber: (a) image and (b) schematic plan view including instrumentation of provided heat and humidity.

MONITORING OF SAMPLES

Samples were continuously monitored, with assessments of strain and examination of cracking occurring at 3-month intervals. External hairline cracking was first observed at an internal expansion of 1100 με, or 0.11 percent deformation for most samples, approximately 430 days after placement in the environmental chamber. All samples were then removed from the environmental chamber to prepare for repair.

Internal deformations over the life of the slabs, rectangular columns, and circular columns are shown in figure 15, figure 16, and figure 17, respectively. In these figures, 100 με is equivalent to 0.01 percent deformation. “Horiz” and “Vert” represent the orientation of each sensor as horizontal or vertical, respectively, and this includes extra sensors placed, which are indicated by “Extra.” Additionally, “Maj” and “Min” represent sensor orientation in the major and minor reinforcement direction of the reinforced slabs. The two slab samples that experienced minimal deformation were selected as control samples and were not repaired.

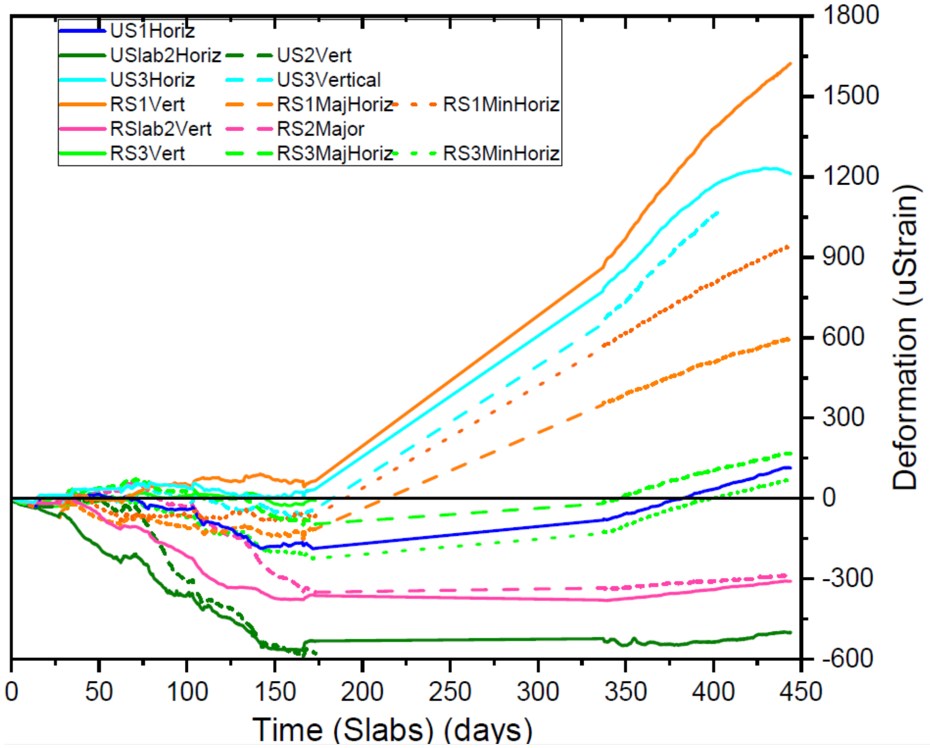

Figure 15. Graph. Internal expansions of slabs.

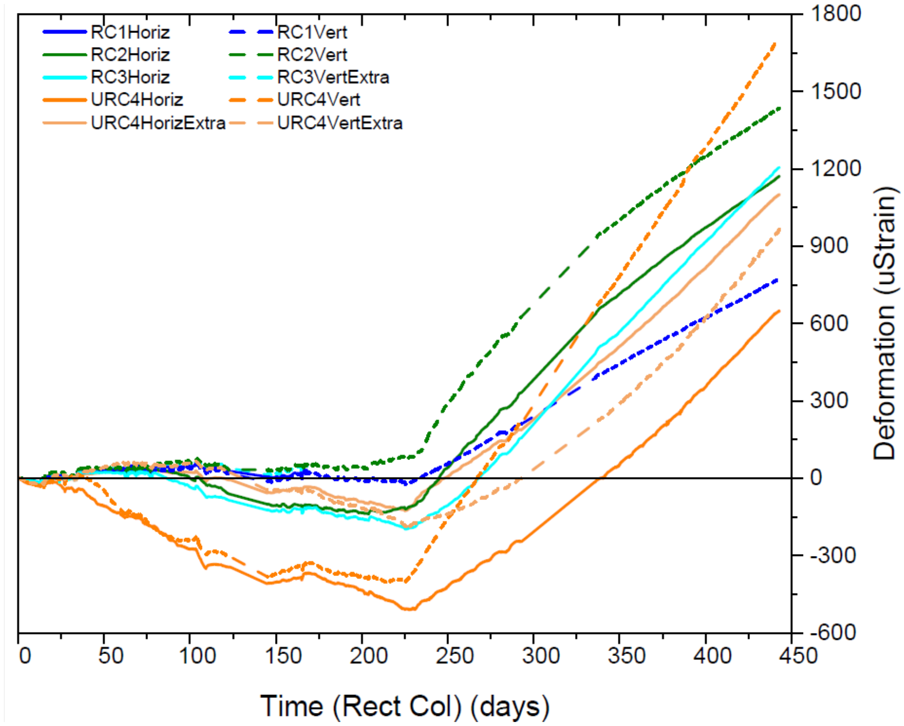

Figure 16. Graph. Internal expansions of rectangular columns.

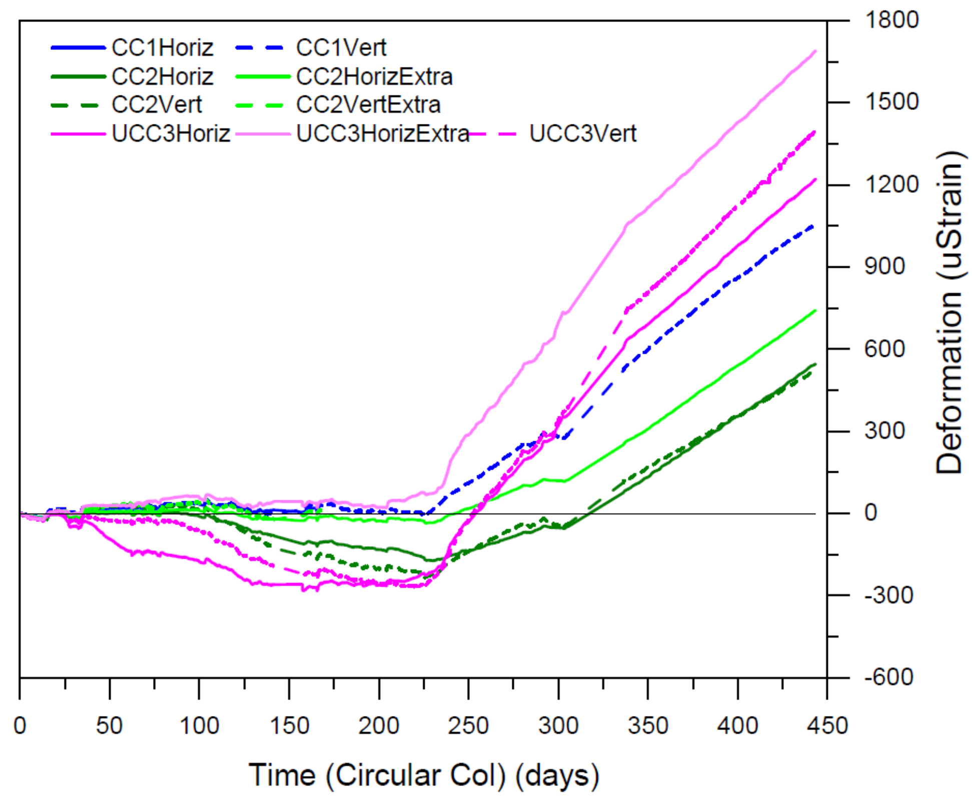

Figure 17. Graph. Internal deformations of circular columns.

Examples of cracking in samples are shown in figure 18(a) in the form of hairline map cracking (visible when sprayed with water) and in figure 18(b), where cracks as large as 0.005 inch (0.127 mm) wide are present. Because these cracks were not visible until this time, they are attributed to be ASR-induced cracks.

Samples were repaired upon visible external damage in order to replicate a realistic repair situation. That is, surface-breaking hairline cracking is typically the first sign that inspectors may note, representing potentially the earliest time that repair may be initiated.

(a) **(b)**

Figure 18. Illustration. Typical surface cracking patterns on ASR-affected reinforced concrete columns when removed from 99 percent RH environmental chamber: (a) hairline map cracking and (b) cracks as wide as 0.005 inch.

REPAIR OF COLUMN AND SLAB SAMPLES

Repair Overview

After 450 days, laboratory-cast samples were removed from the accelerating conditions of the environment chamber and placed in laboratory-room conditions for repair. High-quality images of sample cracks, with resolution of 6000x4000 pixels, were taken as an additional qualitative metric to track the crack development of each sample post-repair. An example of this type of image is provided in figure 19, which shows cracking on the side of a slab sample. The goal of repairing the laboratory-cast samples was to investigate the relative effectiveness of adding coatings and confinement as repair strategies.

Figure 19. Illustration. Example of close-up crack images for future comparison.

The first type of retrofit strategy considered was the application of surface coating. In this research, silane and nanosilica coatings were investigated. Silane coatings are the most common type of repair used for ASR-affected concrete. They create a water vapor barrier to reduce the internal RH. Thus, moisture available for the reaction and gel expansion can be limited, but other avenues for moisture ingress (e.g., from percolation beneath the element, from run-off) must be addressed [31]. The nanosilica coating contains colloidal siliceous particles. These particles have shown to increase internal curing when used as admixtures in new mixture design [32], and they exhibit self-healing properties in cementitious composites [33]. In repairs, they create a surface “clogging” effect against moisture ingress [34]. Details on the coating repairs are given in the subsequent sections of this chapter.

The second retrofit strategy considered was the inclusion of additional confinement via concrete jacketing, which is intended for a more intense level of repairs. Jacketing using various materials (e.g., carbon, steel, and concrete) has proven effective in the retrofitting of columns for various structural applications [35], [36]. Concrete jacketing, specifically, has been shown to be effective in maintaining adequate service life and axial capacity as a retrofit [13], [37]. In some instances, the thickness of normal-strength concrete may need to be large to achieve the confining pressures needed. This is problematic from a construction and economic standpoint. Ultra-high performance concrete (UHPC) was considered for this research effort. UHPC is advantageous in that it has a higher strength as well as a higher ductility. This work specifically used a mixture design from previous research [38] that created UHPC mixture design guidelines for GDOT using local materials.

A test matrix of the specimens that were repaired is provided in table 8, with sample numbers correlating with the sample numbers from the deformation graphs in figure 15, figure 16, and figure 17, as well as the sample nomenclature from table 7. The test series was designed such that the surface coatings treatments were applied to the slabs and the more aggressive chosen repair strategy, jacketing, was applied to the columns. Columns were chosen for jacketing because they are considered a higher priority for maintaining service life. Details on the individual retrofit techniques are given in the next sections.

Table 8. Repair test matrix of laboratory-cast samples.

Unreinforced Slab	Reinforced Slab	Rectangular Column	Circular Column
Control (US 2)	Control (RS 2)	Control (RC 1)	Control (CC 1)
Nanosilica Coating (US 3)	Nanosilica Coating (RS 1)	Nanosilica Coating (RC 3)	Nanosilica Coating (CC 2)
100% Silane (US 1)	100% Silane (RS 3)	UHPC Confinement (RC 2)	UHPC Confinement (CC 3)
N/A	N/A	Unreinforced Control (RC 4)	N/A

Slab Repair

Two slabs were retrofitted with 100 percent silane (US 1 and RS 3), and two slabs were retrofitted with nanosilica (US 3 and RS 1). When silane was used as the repair, a single coat of 100 percent silane was sprayed onto one unreinforced and one reinforced slab. When nanosilica was used as the repair, three coats of the nanosilica coating were sprayed in 24-hour intervals onto separate unreinforced and reinforced slabs, with each coating sprayed until rejection by the surface. In both coating cases, cracks were not treated via caulking or epoxy, allowing better monitoring of crack propagation as a comparison of the two coating treatments. The remaining reinforced and unreinforced slabs were not repaired to provide a form of control sample.

Column Repair

For the coating repair of the columns, the nanosilica coating was applied to one reinforced rectangular column (RC 3) and one reinforced circular column (CC 2) in the same three-coat method as the slabs. The spraying process is shown in figure 20.

Figure 20. Illustration. Spraying nanosilica coating onto laboratory-cast samples.

A reinforced rectangular column (RC 2) and an unreinforced circular column (CC 3) were retrofitted with UHPC jackets. The UHPC mixture had a compressive strength of 21 ksi and a tensile strength of approximately 1.2 ksi [38]. An ANSYS finite element model was completed to determine the thickness required to prevent expansion, which was then increased to the next-size-available “off the shelf” cylindrical formwork. This resulted in a 3-inch-thick jacket. Additionally, to offset stress concentrations at the corners of the rectangular specimen, the corners of the rectangular column were rounded to a 1.5-inch corner radius [39] using an angle grinder with an attached diamond-bit blade, as shown in figure 21.

Figure 21. Illustration. Corner of rectangular column rounded to a 1.5-inch radius.

The columns were sprayed with a silane sealant prior to jacketing in an effort to reduce the permeation of water from the UHPC casting into the column's microstructure. To construct the jacketing, formwork was installed around the columns with a 3-inch gap. The formwork was also lightly sprayed with water in an additional effort to reduce drying shrinkage. The shear mixer (IMER 360) was used to batch the UHPC using the mixture design shown in table 9. Three batches were completed for the circular sample and four for the rectangular sample to accommodate the size of the repair. To avoid creating a cold joint between the time to mix each batch, successive batches were placed in a rotating drum to continue agitation of the UHPC until the total volume was completed mixing. The UHPC was then poured into the formwork via 5-gallon buckets, as shown in figure 22. After casting, the specimen was placed in a moist curing condition at room temperature for 3 days. The two confined samples are shown in figure 23, and 3-inch measurements of the confinements are shown in figure 24.

Table 9. Mixture design for UHPC.

Materials	**Mass (lb/yd^3)**	**Mass Ratio Per Cement Content**
ASTM C595 Type IL Portland limestone cement	1248	1
ASTM C618 Class F fly ash	387	0.31
Metakaolin	100	0.08
Masonry sand (FM = 1.59)	1997	1.6
Superplasticizing admixture	25.7	0.02
Retarding admixture	8.1	0.006
Water	303	0.24
Steel fibers	264.6	0.21

Figure 22. Illustration. Filling confined repair laboratory-cast samples with UHPC.

Figure 23. Illustration. Circular and rectangular confined repair.

(a) **(b)**

Figure 24. Illustration. 3-inch confinement thickness of (a) rectangular column and (b) circular column.

Ongoing Monitoring

The slabs and columns were placed in long-term storage conditions, as shown in figure 25 and figure 26. The slabs were exposed to outdoor conditions to better replicate the environment ASR-affected concrete is subjected to Georgia. The columns were placed back into the environment chamber at a more moderate environment of 85 percent RH and ~24°C temperature condition. This monitoring is still ongoing.

Figure 25. Illustration. Post-repair exposure environment of slabs.

Figure 26. Illustration. Post-repair exposure environment of columns.

Along with high-quality photos of specific crack areas on each sample that were taken prior to repairs, internal expansion via strain gauges and external expansion via insert studs will continue to be monitored for variations in sample expansion and crack development.

CHAPTER 3. REPAIR OF FIELD ASR-AFFECTED CONCRETE

INTRODUCTION

For a field repair study, ASR-affected Jersey concrete traffic barriers were selected as the specimen. Jersey barriers are located on the ground and are only a few feet tall with adequate shoulder width from traffic, which allows for ease of surface prep and product application compared to other structures, such as columns, which would necessitate a means of vertical travel by ladder or lift. Coating materials were again explored as a repair strategy in this phase of the research.

Silane coatings reduce moisture ingress into concrete surfaces. Unlike paints that form a surface film, silane molecules are small enough to penetrate the concrete's pores and cracks where they react with calcium hydroxide, forming a microscopic, water-repellent resin. This resin acts like a barrier, repelling water molecules and significantly reducing moisture ingress. This approach offers several advantages. Because the silane reacts within the concrete, it creates an effective semipermeable membrane, allowing water vapor to leave the microstructure while still preventing liquid water from entering, with reported depths of at least 3 inches [6], [11]. Additionally, silane treatments are typically colorless and do not alter the concrete's appearance. The primary benefit of reduced moisture in concrete is improved durability, including slowing the progression of ASR. It is important to note that silane treatments are not permanent and may require periodic reapplication, and their effectiveness can be influenced by the concrete's porosity and surface preparation. Silane coatings have been demonstrated to offer protection to ASR-affected concrete surfaces in numerous studies [5], [6], [24], [40], and they were recommended by experts consulted in the field of concrete repair, including Prof. Jason Ideker, Dr. Jonah Kurth, and Dr. Anthony Bentivegna.

A strip of seven 25-ft-long barriers with initial apparent ASR damage were located on the northbound Buford Spring Connector (State Route 13) near Peach Street NE in Atlanta, Georgia (approximately 33.800°N, −84.389°W). Figure 27 contains the geographical location of the barriers. Figure 28 shows the initial surface. Map cracking that is typical of ASR damage can be seen on the barriers with what was also believed to be gel exudation. Because of the uniform level of damage along each barrier, it is believed that they were all placed at the same time with similar mixture designs.

Figure 27. Illustration. Geographical location of barriers.

Figure 28. Illustration. Surface of barriers.

CHARACTERIZATION

To confirm if ASR was, in fact, the cause of the concrete's damage, petrography using uranyl acetate to highlight gel on a sample was performed in accordance with ASTM C856-14 [20] (Standard Practice for Petrographic Examination of Hardened Concrete) Appendix X1. The concrete sample under white light is shown in figure 29(a). Figure 29(b) shows a crack in an aggregate as well as an alkali-rich reaction product around an aggregate. Reaction products were also observed in voids, and the results of this petrographic characterization provided sufficient proof of ASR-affected concrete.

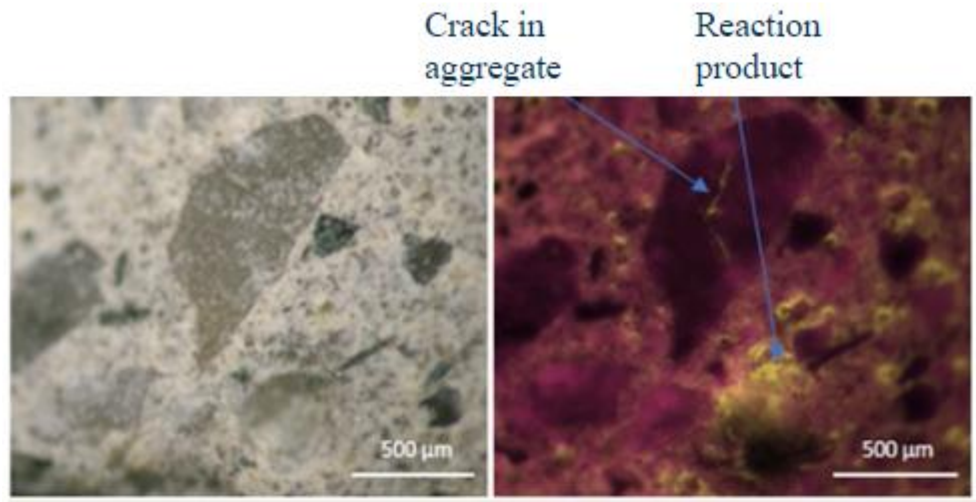

(a) **(b)**

Figure 29. Illustration. Barrier concrete core cross section under 20× magnification with (a) white light and (b) UV lighting.

REPAIR OF BARRIERS

Within previously tested surface coatings, silanes have been observed to be most successful in mitigating future expansion of ASR-affected concrete [5], [10], [41], although discrepancies exist as to what base of silane is most effective. A test matrix was designed to explore the various silane sprays, as well as a new proprietary slurry treatment with the potential to mitigate ASR, which was already observed when it was added to new concrete susceptible to ASR-damage [42]. The barriers were divided into thirds with a control group in the middle, which is represented by a schematic of Barrier A in figure 30. The test matrix details are provided in table 10. Water-based silane, alcohol-based silane, and 100 percent silane were tested, and three variations of the slurry treatments were also included. For the silanes, caulking was applied to cracks greater than 0.03 inch either before or after application of the silane as another variable tested in the matrix.

Table 10. Repair test matrix for field ASR-affected concrete barriers.

Barrier Name	Product Type	Flexible Caulking
A1	Water Based Silane	Before
A2	Control	None
A3	Water Based Silane	After
B1	Alcohol Based Silane	Before
B2	Control	None
B3	Alcohol Based Silane	After
C1	100% Silane	Before
C2	Control	None
C3	100% Silane	After
D1	Water Sealer	Before
D2	Control	None
D3	Water Sealer	After
E1	100% Silane	N/A
E2	Control	N/A
E3	Slurry Product 1	N/A
F1	100% Silane	N/A
F2	Control	N/A
F3	Slurry Product 2	N/A
G1	100% Silane	N/A
G2	Control	N/A
G3	Slurry Product 3	N/A

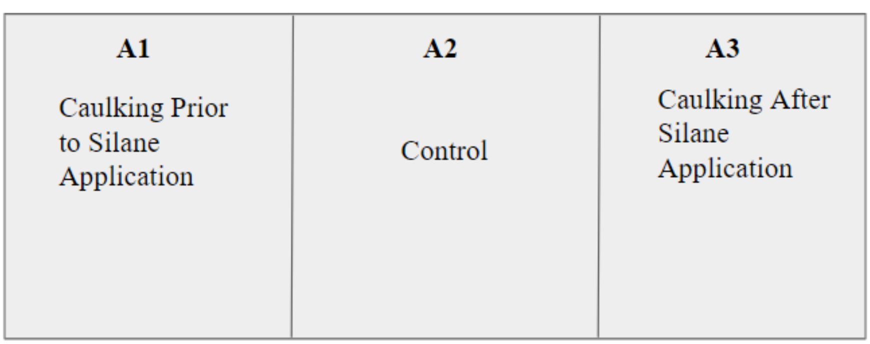

Figure 30. Illustration. Example schematic of repair division per barrier.

External expansion studs were also installed to monitor expansion using a multilength strain gauge. These gauges were checked periodically on days with consistent temperatures. Machine screws were inserted into the expansion studs between readings to avoid dirt buildup that could impact data collection.

Two cores were taken per specimen. After cores were taken, surface preparation and application of the products to the barriers began. All barriers were first pressure washed (figure 31). The color difference between the initial condition and post–pressure washing is believed to be due to biofilm and oil residue from form release oils that were explored in a previous GDOT project [43]. Core holes were then filled with spray foam to allow continued expansion inside the hole (and therefore not provide artificial restraint) and topped off with repair grout to prevent excess moisture from entering.

Where indicated in the test matrix, cracks of greater than roughly 0.03 inch were caulked prior to silane application. Silanes were then sprayed using a fan-tip non-atomizing metal sprayer, starting from the bottom and moving up in horizontal layers and dosed at the manufacturer’s recommendation for each silane type. This process is shown in figure 32. In relevant sections, applicable cracks were then caulked after silane spraying.

Figure 31. Illustration. Pressure washing barriers.

Figure 32. Illustration. Spraying a barrier with silane coatings.

The three slurry treatment products were then applied on Barriers E3, F3, and G3. Cracks large enough were grounded to wider opening sections using a cutoff tool and diamond bit. A grout-based product from the same manufacturer as the slurry-based products was then applied to fit into this larger opening. Once the product was cured, powder and water were mixed by volume on-site using a volumetric flask. The slurry was then applied using a masonry brush in a circular motion with enough concentration to ensure the minimum desired thickness. This process is shown in figure 33. After application, a plastic tarp was placed over the barriers to allow curing. Following this, a final water-proof silane/siloxane spray (also provided by the manufacturer) was applied to the now slurry-covered surface.

Figure 33. Illustration. Application of slurry coating.

Final images of barriers repaired with silane spray and caulking and with the slurry coating are shown in figure 34 and figure 35, respectively. Expansion anchors that protrude from the surface from previous coring are still intact for any needed future coring.

Figure 34. Illustration. Post-repair of silane-treated Barrier A1.

Figure 35. Illustration. Post-repair of slurry-coated Barrier F3.

ONGOING MONITORING

Barriers are currently being monitored for external expansion using the installed studs. It is important that the ambient temperature be similar to the initial readings, so there are seasonal limitations on when new deformation readings can be taken. External deformation measured to date (approximately 50 weeks after repair) is included in figure 36. Figure 37 includes the external deformations of solely barriers that test repair success of silanes against middle (control) sections (along with order of caulking cracks before or after silane application). Figure 38 includes the external deformation of solely barriers that test repair success of slurries against 100 percent silane coatings to the control (middle) sections. Although control sections (indicated by dashed lines) are included for comparison, the order of caulking and silane application for Barriers A–C is not yet distinguished by color for better readability at this stage. An overall slight contraction is observed in all barriers, likely due to temperature differences since the initial readings. The magnitude of this change is within the margin of error for the measuring instruments, so no conclusions can be drawn yet about the treatments' effectiveness. Meaningful differences in expansion readings are expected to be visible within two years of initial application (i.e., Spring 2025).

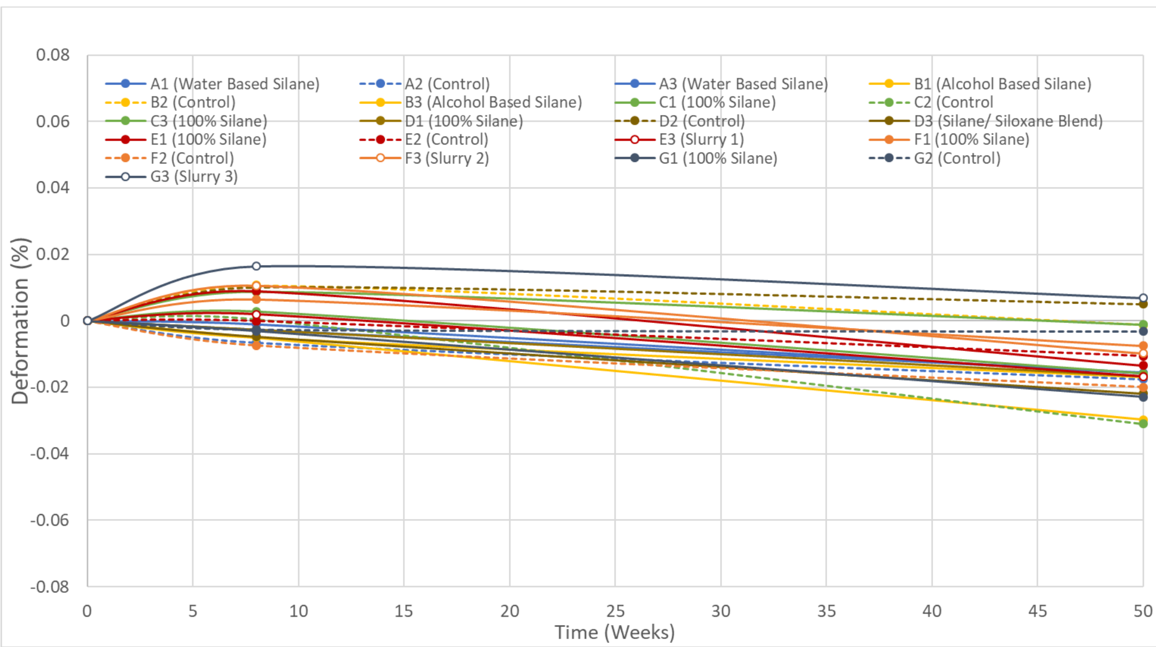

Figure 36. Graph. External deformation of Jersey barriers.

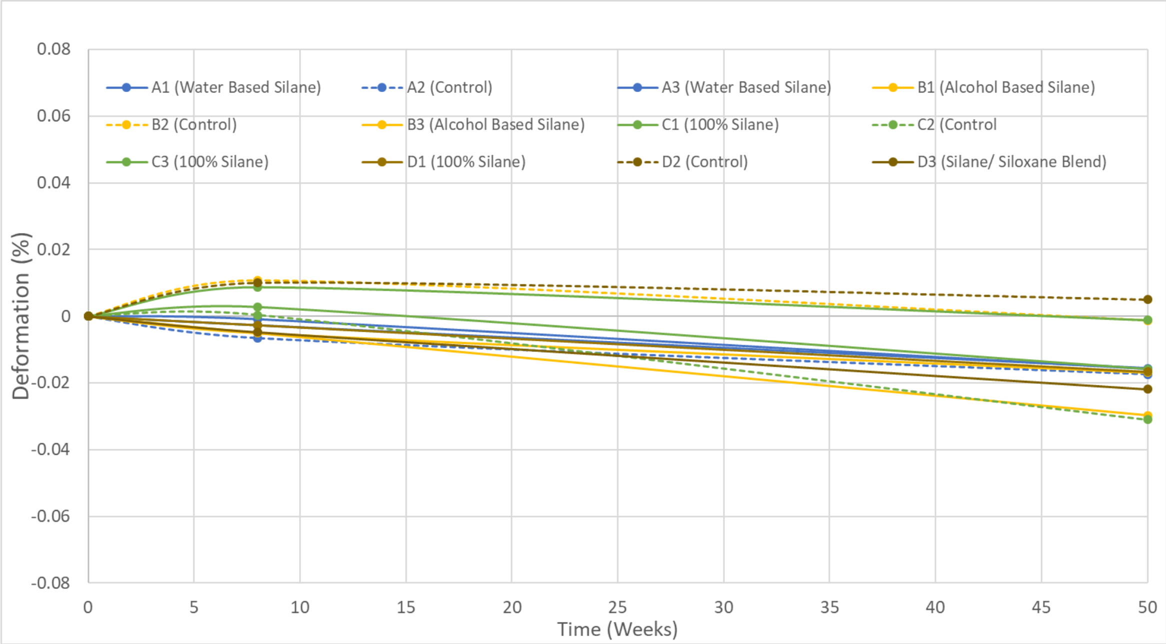

Figure 37. Graph. External deformation of silane-repaired Jersey barrier sections.

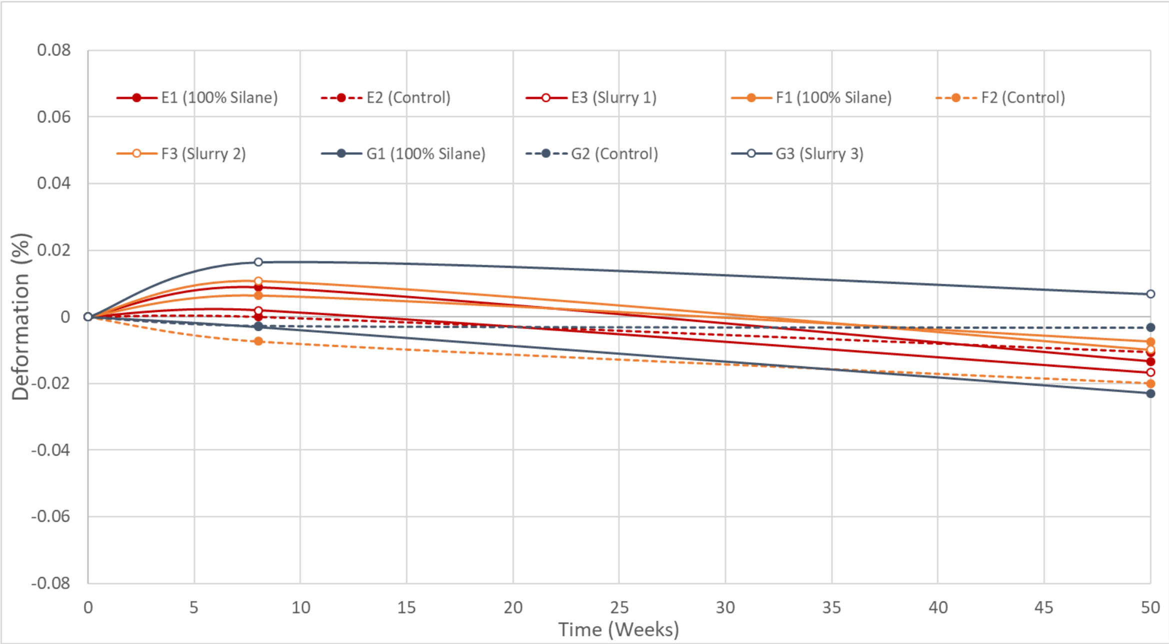

Figure 38. Graph. External deformation of slurry-repaired Jersey barrier sections.

Photos of each section taken post-repair can be qualitatively compared to future pictures to assess major crack propagation and potential further gel exudation. Selecting an appropriate moisture management technique for concrete repairs requires balancing internal and external moisture considerations. Silane treatments offer a more direct pathway for internal moisture egress due to their high surface area. However, slurry coatings, with their ability to fill microcracks, are expected to outperform in mitigating external water ingress and the resultant expansion, thanks to the combined effects of mechanical protection and the additional silane/siloxane layer. It is still anticipated that the silanes will mitigate future expansions, but continued monitoring will dictate which type of silane performs best.

CHAPTER 4. RECOMMENDATIONS AND CONCLUSIONS

RECOMMENDATIONS FOR REPAIR

Formulation of repair recommendations for ASR-affected concrete in Georgia remains contingent upon results from ongoing monitoring. However, by synthesizing the latest published research on ASR mitigation strategies in the context of preliminary data collected in this investigation, some preliminary guidance can be generated. Specifically, the FHWA has published several reports on ASR identification, prognosis, and repair [7], [11], [44] that, along with other published sources, can inform practices recommended in this state.

Because the severity of ASR damage directly correlates with the extent of mechanical property loss and crack development, repair recommendations should be stratified based on the relative degrees of observed ASR damage. Although AASHTO tools, such as Pontis software and the *Guide Manual for Bridge Element Inspection* [45], help inspectors recognize signs of ASR damage, more specific guidance is provided in the FHWA document developed by Thomas et al. [46]. This document associates ASR-related defects including map cracking and misalignment, which are not well tracked in bridge inspection systems, and uses specific criteria to quantify the condition state for bridges (table 10). Table 11 provides guidance in quantifying distress for the assignment of the condition state for bridges. Table 12 and table 13 provide similar guidance for pavements.

Table 11. Recommended defects and condition states for element types potentially affected by ASR. [46]

Defect	Condition State 1	Condition State 2	Condition State 3	Condition State 4
Map cracking	None–hairline	Narrow size or density or both	Medium size or density or both	The condition is beyond the limit state of Condition State 3, warrants a structural review to determine the strength or serviceability of the element or bridge, or both
Aligned cracking	None–hairline	Narrow size or density or both	Medium size or density or both	
Gel exudation	None	Moderate	Severe (with gel staining)	
Relative dislocation/misalignment	None	Tolerable	Approaching or exceeding limits (including causing local crushing)	

Table 12. Recommended defects and defect description for element types potentially affected by ASR. [46]

Defect	Hairline–Minor	Narrow–Moderate	Medium–Severe
Map cracking	• Crack width: <0.0625 inch (1.6 mm) • % Map cracking: <5%	• Crack width: 0.0625–0.1250 inch (1.6–3.2 mm) • % Map cracking: 5%–25%	• Crack width > 0.1250 inch (3.2 mm) • % Map cracking: >25%
Aligned cracking	Crack width: <0.0625 inch (1.6 mm)	Crack width: 0.0625–0.1250 inch (1.6–3.2 mm)	Crack width: >0.1250 inch (3.2 mm)
Gel exudation	None	Gel visible on surface (<20% of concrete surface, with no buildup of gel)	Gel buildup on surface (>20% of concrete surface), typically at or near cracks; gel staining visible (especially once structure dries after a rain event)
Relative dislocation/ misalignment	None	Tolerable (movement is visible but no loss of clearance, exudation of sealants at joints, or local crushing)	Movement is visual, with loss of clearance, exudation of sealants at joints, or local crushing

Table 13. Recommended distress and condition states for pavements potentially affected by ASR. [46]

Distress	Condition State			
	1	2	3	4
Map cracking	None–hairline	Narrow size or density or both	Medium size or density or both	The condition is beyond the limit state of Condition State 3, warrants a structural review to determine the strength or serviceability of the element or pavement, or both
Joint sealant failure	None	Moderate	Severe	
Joint deterioration	None	Moderate	Severe	
Popouts	None	Moderate	Severe	

Table 14. Recommended distress and distress description for pavements potentially affected by ASR. [46]

Distress	Hairline–Minor	Narrow–Moderate	Medium–Severe
Map cracking	• Crack width: <0.0625 inch (1.6 mm) • % Map cracking: <5%	• Crack width: 0.0625–0.1250 inch (1.6–3.2 mm) • % Map cracking: 5%–25%	• Crack width: >0.1250 inch (3.2 mm) • % Map cracking: >25%
Joint sealant failure	Joint sealant failure in less than 10% of joints.	Joint sealant failure in 10%–50% of joints.	Joint sealant failure in greater than 50% of joint
Joint deterioration	None or only minor cracking near corners/joints	Wide, open cracks exist and mass loss has occurred in joint region (less than 5% of joints). No patching applied.	Wide, open cracks and mass loss has occurred in joint region (greater than 5% of joints). Patching has been applied.
Popouts	None	Popouts isolated and few (less than 1 popout per 10 ft)	Popouts prevalent (greater than 1 popout per 10 ft)

* Popout data are generally not collected and are not included in long-term pavement performance (LTPP). Estimates are shown in parentheses.

The following sections summarize repair options, based on relative amounts of damage, with the least severe manifestations addressed first. AASHTO [45] provides guidance (see table 15) for repair of bridge elements based on the condition state. A similar approach is recommended for pavements. Early detection is also recommended in condition states 1 and 2 whenever possible.

Table 15. Feasible action for defects. [46]

Condition State			
1	**2**	**3**	**4**
• Do nothing • Protect	• Do nothing • Protect	• Do nothing • Protect • Repair • Rehab	• Do nothing • Rehab • Replace

Concrete with Minimal Damage: Silane Coatings

Minimal damage (or "Fair condition") is defined as "…minor, moderate, and severe defects are present but with no significant section loss" [46] and can also best be associated with Condition States 1 and 2 from the previous section in most cases. For concrete with minimal ASR damage that does not need external strengthening to maintain service life, repairs can focus on mitigating future expansion. As stated previously, silanes are well established in the research to minimize further degradation by lowering the internal RH of the concrete's microstructure and thus lowering a necessary reactant for ASR gel and expansion. As a general form, silanes (but not siloxanes or other similarly derived molecules) have been effective in mitigating expansion 25 years after application against control samples in the longest running test of silanes available [40]. In similar work of silane application as a general form of improving concrete durability to ion ingress, silanes were effective for at least 12 years [47]. Different degrees of effectiveness have been observed with specific silane bases (i.e., alcohol base, water base, and 100 percent silane), which prompts their comparison in this investigation. In general, it is anticipated that a higher silane concentration provides more effective mitigation.

Prior to the application of the silane, it is recommended to treat cracks larger than hairline (approximately 0.016 inch) to best reduce moisture ingress. This can be accomplished by using a flexible caulk, such as in [11].

Concrete with Minimal to Moderate Damage: Nanosilica and Slurry Coatings

For concrete exposed to ASR damage with more prominent map cracking where it may be difficult to effectively fill all cracks, nanosilica or slurry coatings are recommended. This would correspond to Condition States 1–3, potentially.

Because moisture can enter through thin hairline cracks common with map cracking, and covering or filling all hairline cracks is not feasible, the potential ability for nanosilica-containing or crystalline-based slurry coatings to “heal” these cracks at the microscale [33], [42] make for the most appropriate recommendation. For ASR-affected concrete in an environment where added physical protection is needed (such as a region where the concrete may be exposed to deicing salts), application of the slurry coating is recommended, although more labor-intensive.

Concrete with Medium to Severe Damage: Confinement

For concrete exposed to higher ASR damage where significant mechanical loss is present or for a structure more critical to maximize service life, the risk of structural failure is a higher concern and thus repair that includes mechanical strengthening and physical protection is needed. Confinement offers the most efficient method of strengthening ASR-damaged concrete. Currently, confinement of ASR-affected concrete has been completed using several materials, most notably normal reinforced concrete [13] and fiber-reinforced polymers (FRP) [12], [48]. These two materials can be successful in confining ASR-affected concrete, but limitations exist. For example, normal concrete needs significant additional space for confinement to achieve adequate provided strengths, particularly if reinforcement is added for appropriate cover depths. For FRP confinement, a weak bond interface has proven to be a challenge as a failure mode [48], and because the material is thin, it relies on low redundancies if failure were to happen. For the first time, UHPC was evaluated for confinement of ASR-affected large-scale concrete and reinforced concrete elements in this investigation. Fiber-reinforced UHPC offers sufficient strain-hardening capacity necessary to confine expanding concrete, and this can be achieved with a lesser thickness of materials than if using conventional reinforced concrete, which is a new approach to confining ASR-affected concrete on a large scale. At the same time, the applied UHPC layer can resist any crack propagation.

UHPC thickness should be determined through model-based predictions of ASR-induced tensile stress that the confinement must resist. Residual expansion studies [49], [50], performed by storing cored samples in an accelerating environment, can be helpful in assessing potential for future expansion. Additionally, it is recommended to treat the ASR-damaged concrete surface with a silane or waterproof coating prior to UHPC confinement to prevent moisture penetration from the UHPC into the element. In special cases were confinement may not be possible such as a tunnel, unique repairs must be explored on a case-by-case basis.

Summary

Notable advantages and disadvantages for each repair strategy are summarized in table 16. It is important to note that repair requires fewer resources and is more effective when treatment occurs as soon as possible to limit further damage.

Table 16. Advantages and disadvantages of each repair type.

Repair	Initial Concrete Damage	Advantages	Disadvantages
Silane coating	Minimal–moderate	• Easy to apply • Well established effectiveness in literature	• Loses effectiveness on concrete with large depths due to penetration depth of coating
Nanosilica coating	Minimal–moderate	• May provide crack filling at the microscale	• Limited research available
Slurry coating	Moderate	• Provides physical protection • May provide crack filling at the microscale	• More labor-intensive than other coatings • Limited research available
UHPC confinement	Moderate–severe	• Provides strengthening of affected element • Design can be validated through modeling	4. Most labor- and resource-intensive

RECOMMENDATIONS FOR FUTURE WORK

Introduction

As is clear from the previous section, repair of ASR-affected concrete is easier to accomplish and more effective the sooner damage is detected. Unfortunately, by the time visible damage is evident as surface-breaking cracks, permeability is likely increased, increasing the risk for other forms of damage to initiate. Further, mechanical properties of the concrete may have already been significantly reduced. Loss of mechanical properties make repair challenging, depending on the structure type, because not only does the ASR need to be mitigated through moisture control but strengthening of the damaged concrete may also be required. To better prevent the need for more labor-intensive and costly repairs, it is recommended to explore further work into early detection of ASR-affected concrete by nondestructive testing and laboratory characterization methods.

Micro X-ray Fluorescence

X-ray fluorescence (XRF) spectroscopy is a characterization technique that combines high magnification imaging with elemental composition analysis**.** It functions by irradiating the sample with an X-ray source and interpreting the backscattered X-rays, which are uniquely dispersed based on the stimulated electron transitions within the constituent elements [51]. Micro-XRF (μXRF) is a spatially resolved variant of XRF, capable of achieving spot sizes as small as 20 μm. This technique has demonstrated success in characterizing other forms of concrete deterioration, such as sulfate attack [52]. Additionally, preliminary investigations suggest its potential for characterizing ASR damage in concrete [53]. For example, figure 39 depicts several characteristics of ASR damage at the microscale level from a concrete core. Specifically, figure 39(c) highlights

ASR gel at the tip of two aggregates (at the bottom corners of the image) due to high concentrations of potassium.

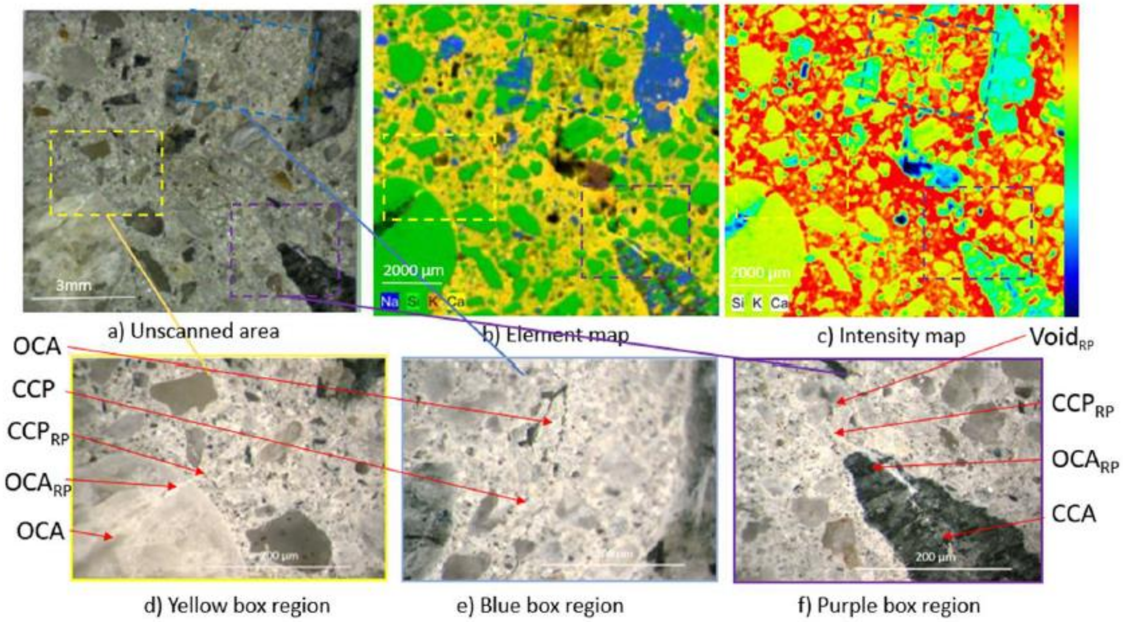

Figure 39. Illustration. Characterization of ASR Damage: (a) Square B9 of Core C2R under mosaic viewing of µXRF; (b) element map of B9 with Si, Na, K, and Ca turned on; (c) intensity map of the combined elements Si, K, and Ca with scaling of blue (lowest intensity) to red (highest intensity); (d) zoomed in image of the yellow box from (a); (e) zoomed in image of the blue box from (a); (f) zoomed in image of the purple box from (a) [53].

Further research utilizing µXRF could lead to the development of methods for earlier detection of ASR damage based on small core samples, providing another method for concrete inspection.

Nondestructive Testing

Additionally, advanced nondestructive testing (NDT) and evaluation (NDE) techniques are powerful tools for internal defect detection within concrete. In particular, nonlinear acoustics or ultrasound have been demonstrated to be particularly sensitive to microscale damage characteristic to ASR damage and other forms of concrete distress, and these methods can be applied to both laboratory samples (including cores) and in situ concrete elements, pavements, and structures [54]. In particular, noncollinear wave mixing holds promise for ASR damage assessment as it exhibits minimal signal scattering from inherent concrete inhomogeneity [55], [56]. Preliminary work with the setup shown in figure 40 has also shown promise in identifying ASR within a large-scale sample exposed to ASR damage throughout.

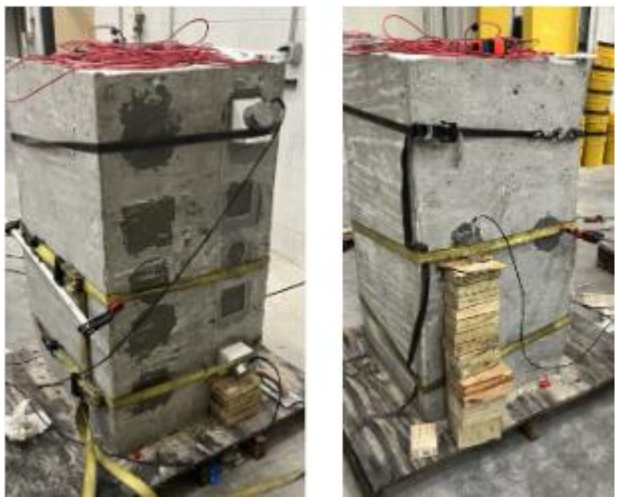

Figure 40. Illustration. Front (left) and back (right) views of ASR-affected concrete sample under NDT ultrasonic noncollinear wave mixing testing.

Ultrasonic NDT has the potential to not only confirm the presence of ASR damage but also quantify its severity within concrete elements. The development of such advanced characterization methods can facilitate earlier identification of the need for repairs, quantitatively assess the rate of damage progression, and guide the selection of appropriate repair strategies based on the quantified level and rate of ASR damage.

CONCLUSIONS

ASR damage poses an increasing threat to the service life of the existing concrete infrastructure, including in Georgia**.** This detrimental reaction compromises structural integrity by reducing mechanical properties and increasing permeability through expansion-induced cracking. Timely repairs are crucial to extend service life. While existing literature has explored various repair solutions, inconsistencies in reported success and the emergence of new technologies necessitate a reevaluation of repair options, particularly considering the extent of damage for optimal efficiency.

This report details an investigation utilizing large-scale laboratory-cast specimens replicating Georgia's concrete structural elements, bridge decks, and pavements in terms of mixture design, material sourcing, and structural design. The repair strategies employed on these specimens included coatings and confinement, with the latter representing a more resource-intensive but aggressive approach. Notably, this research explored the application of novel repair technologies, including nanosilica and UHPC, to ASR-affected concrete.

Field-extracted ASR-damaged Jersey traffic barriers were also included in the study, with a focus on coating repairs using silanes and slurries. Given the reported inconsistencies in the performance of various silane base materials, expansion data from these barriers will be leveraged to identify appropriate silane formulations for mitigating ASR-induced expansion. Additionally, slurry coatings were investigated as a novel technology with the potential to prevent further water ingress through the filling of microcracks.

While long-term data are necessary for definitive recommendations on each repair solution, initial suggestions were formulated based on anticipated outcomes and recent relevant literature.

ACKNOWLEDGMENTS

The authors gratefully acknowledge the technical advice and expertise of Peter Wu, Samuel Benford, Steve Gaston, Jason Waters, Sephara Raymond, and Brennan Roney from GDOT, as well as the financial support for this research. In addition, the efforts of Georgia Tech undergraduate research assistants Paul Lee, Evan Young, Mariyam George, Jimmy Rivas-Granados, and Caroline Fjeran contributed to this research.

REFERENCES

1. K. J. Folliard, M. D. A. Thomas, B. Fournier, J. H. Ideker, and B. East, “Treatment of Structures with Alkali-Silica Reactive Distress with Lithium Nitrate: Case Studies,” in *TRB Annual Meeting*, National Academies, Washington D.C., 2009.
2. A. Bentivegna, E. R. Giannini, and K. J. Folliard, “Electrochemical repair Use of electrochemical migration to mitigate alkali-silica reaction in large scale concrete structures,” in *Concrete Solutions*, Taylor & Francis Group, 2012.
3. K. J. Folliard, M. D. A. Thomas, and K. E. Kurtis, “Guidelines for the Use of Lithium to Mitigate or Prevent Alkali-Silica Reaction (ASR),” Federal Highway Administration, Washington, DC, National Research Council, FHWA-RD-03-047, 2003.
4. J. Pednault, “Development of testing and analytical procedures for the evaluation of the residual potential of reaction, expansion, and deterioration of concrete affected by ASR,” M.Sc. Thesis, Université Laval, Québec City, 1996.
5. E. Giannini, A. Bentivegna, and K. Folliard, “Coatings and Overlays for Concrete Affected by Alkali-Silica Reaction,” presented at the Concrc - Proceedings of Concrete Solutions, 4th International Conference on Concrete Repair, Sep. 2011. doi: 10.1201/b11585-116.
6. R. Deschenes, E. R. Giannini, T. Drimalas, B. Fournier, and W. M. Hale, “Mitigating Alkali-Silica Reaction and Freezing and Thawing in Concrete Pavement by Silane Treatment,” *ACI Mater. J.*, vol. 115, no. 5, Sep. 2018, doi: 10.14359/51702345.
7. K. D. Basham, “Evaluation of Treatment Options for ASR-Affected Concrete: Final Report,” Wyoming, United States, FHWA-WY-10/01F, 2009. [Online]. Available: https://rosap.ntl.bts.gov/view/dot/17647
8. R. N. Swamy, “Assessment and rehabilitation of AAR-affected structures,” *Cem. Concr. Compos.*, vol. 19, no. 5–6, pp. 427–440, Jan. 1997, doi: 10.1016/S0958-9465(97)00035-8.
9. M. R. Sakr, M. T. Bassuoni, and A. Ghazy, “Durability of Concrete Superficially Treated with Nano-Silica and Silane/Nano-Clay Coatings,” *Transp. Res. Rec. J. Transp. Res. Board*, vol. 2675, no. 9, pp. 21–31, Sep. 2021, doi: 10.1177/0361198120953160.
10. R. A. Deschenes, “Mitigation and Evaluation of Alkali-Silica Reaction (ASR) and Freezing and Thawing in Concrete Transportation Structures,” Ph.D. Thesis, University of Arkansas, Fayetteville, 2017.
11. M. D. A. Thomas, K. J. Folliard, B. Fournier, P. Rivard, and T. Drimalas, “Methods for Evaluating and Treating ASR-Affected Structures: Results of Field Application and Demonstration Projects –,” Federal Highway Administration, Washington, DC, FHWA-HIF-14-0002, 2013.

12. R. Haddad, M. J. Shannag, and M. Al-Hamouth, “Repair of Reinforced Concrete Beams Damaged by Alkali-Silica Reaction,” *Aci Struct. J.*, vol. Vol. 105, pp. 145–153, Mar. 2008.

13. K. G. Talley, “Assessment and strengthening of ASR and DEF affected concrete bridge columns,” Ph.D. Thesis, The University of Texas at Austin, Austin, 2009.

14. Z. D. Webb, “Experimental investigation of ASR/DEF-induced reinforcing bar fracture,” MS Thesis, The University of Texas at Austin, Austin, Texas.

15. K. Tosun, F. Burak, and B. Bulent, “Effectiveness of Alkyl Alkoxy Silane Treatment in Mitigating Alkali-Silica Reaction,” *ACI Mater. J.*, vol. 105, no. 1, pp. 20–27, 2008.

16. E. R. Giannini, “Evaluation of concrete structures affected by alkali-silica reaction and delayed ettringite formation,” Ph.D. Thesis, The University of Texas at Austin, Austin, Texas, 2012.

17. Georgia Department of Transportation, “QPL 2 Coarse Aggregate Sources.” Office of Materials and Testing, 2024.

18. Georgia Department of Transportation, “QPL 1 Concrete Sand Sources.” Office of Materials and Testing, 2024.

19. “ASTM C1260 Standard Test Method for Potential Alkali Reactivity of Aggregates (Mortar-Bar Method).” West Conshohocken, PA, 2021. doi: 10.1520/C1260-22.

20. “ASTM C856-14 Practice for Petrographic Examination of Hardened Concrete.” ASTM International, West Conshohocken, PA, 2014.

21. J. F. Muñoz, C. Balachandran, and T. S. Arnold, “New Turner-Fairbank Alkali-Silica Reaction Susceptibility Test for Aggregate Evaluation,” *Transp. Res. Rec.*, vol. 2675, no. 9, pp. 798–808, Sep. 2021, doi: 10.1177/03611981211004584.

22. “ASTM C1293-20a, Standard Test Method for Determination of Length Change of Concrete Due to Alkali-Silica Reaction.” West Conshohocken, PA, 2020. [Online]. Available: https://www.astm.org/c1293-20a.html

23. “Standard Specifications Construction of Transportation Systems Section 500 Concrete Structures.” 2021.

24. R. D. Lute, K. J. Folliard, T. Drimalas, and C. K. Rust, “COATINGS AND SEALERS FOR MITIGATION OF ALKALI-SILICA REACTION AND/OR DELAYED ETTRINGITE FORMATION”.

25. Z. Li, H. Rashidian-Dezfouli, and P. R. Rangaraju, “Application of UHPC in Mitigation of ASR Distress in Existing Concrete Structures,” *PCI*, 2016.

26. S. H. Diab, A. M. Soliman, and M. Nokken, “Exterior strengthening for ASR damaged concrete: A comparative study of carbon and basalt FRP,” *Constr. Build. Mater.*, vol. 235, p. 117435, Feb. 2020, doi: 10.1016/j.conbuildmat.2019.117435.

27. B. Mota, T. Matschei, and K. Scrivener, “Impact of NaOH and Na2SO4 on the kinetics and microstructural development of white cement hydration,” *Cem. Concr. Res.*, vol. 108, pp. 172–185, Jun. 2018, doi: 10.1016/j.cemconres.2018.03.017.

28. J. B. Mander, M. J. N. Priestley, and R. Park, “Theoretical Stress-Strain Model for Confined Concrete,” *J. Struct. Eng.*, vol. 114, no. 8, pp. 1804–1826, Aug. 1988, doi: 10.1061/(ASCE)0733-9445(1988)114:8(1804).

29. M. Allford Therese, “Expansion Behavior of Reinforced Concrete Elements Due to AlkaliSilica Reaction,” MS Thesis, The University of Texas at Austin, Austin, Texas, 2016.

30. P. Li, N. Tan, X. An, K. Maekawa, and Z. Jiang, “Restraint Effect of Reinforcing Bar on ASR Expansion and Deterioration Characteristic of the Bond Behavior,” *J. Adv. Concr. Technol.*, vol. 18, no. 4, pp. 192–210, Apr. 2020, doi: 10.3151/jact.18.192.

31. Edward McGettigan, “Silicon-Based Weatherproofing Materials,” *Concr. Int.*, vol. 14, no. 6, pp. 52–56, Jun. 1992.

32. Lyles School of Civil Engineering, Purdue University, West Lafayette, IN 47907-2051, USA *et al.*, “Investigation of Internal Curing Efficacy of Portland Cement Concrete incorporated with Colloidal Nano Silica,” *ES Mater. Manuf.*, 2022, doi: 10.30919/esmm5f798.

33. C. Huang, Y.-F. Su, P. Baah, T. Nantung, and N. Lu, “Investigation of medium-term self-healing performance of strain-hardening cementitious composites incorporated with colloidal nano silica,” *Constr. Build. Mater.*, vol. 348, p. 128687, Sep. 2022, doi: 10.1016/j.conbuildmat.2022.128687.

34. B. El Haddaji *et al.*, “Nanosilica-based post-treatment of hardened cement-based materials: The underlying physics,” *Cem. Concr. Res.*, vol. 171, p. 107211, Sep. 2023, doi: 10.1016/j.cemconres.2023.107211.

35. S. Raza, M. K. I. Khan, S. J. Menegon, H.-H. Tsang, and J. L. Wilson, “Strengthening and Repair of Reinforced Concrete Columns by Jacketing: State-of-the-Art Review,” *Sustainability*, vol. 11, no. 11, p. 3208, Jun. 2019, doi: 10.3390/su11113208.

36. Y. Xiao and H. Wu, “Retrofit of Reinforced Concrete Columns Using Partially Stiffened Steel Jackets,” *J. Struct. Eng.*, vol. 129, no. 6, pp. 725–732, Jun. 2003, doi: 10.1061/(ASCE)0733-9445(2003)129:6(725).

37. M. Nomura, A. Komastubara, K. Fujimoto, and K. Torii, “Evaluation of maintenance methods for ASR-damaged structures in Hokuriku district, Japan”.

38. L. K. Stewart, L. Kahn, K.E. Kurtis, G., Loreto., “Development of GDOT Ultra-High Performance Concrete for Bridge Deck Closure Pours,” FHWA-GA-22-1801, Apr. 2022. [Online]. Available: https://rosap.ntl.bts.gov/view/dot/68404

39. L.-M. Wang and Y.-F. Wu, “Effect of corner radius on the performance of CFRP-confined square concrete columns: Test,” *Eng. Struct.*, vol. 30, no. 2, pp. 493–505, Feb. 2008, doi: 10.1016/j.engstruct.2007.04.016.

40. M. Champagne, M. Roy-Tremblay, B. Fournier, J. Duchesne, and B. Bissonnette, “Long-term effectiveness of sealers in counteracting alkali–silica reaction in

highway median barriers exposed to wetting and drying, freezing and thawing, and de-icing salts," Universite Laval, 2016.

41. M.-A. Bérubé, D. Chouinard, M. Pigeon, J. Frenette, M. Rivest, and D. Vézina, "Effectiveness of sealers in counteracting alkali-silica reaction in highway median barriers exposed to wetting and drying, freezing and thawing, and deicing salt," *Can. J. Civ. Eng.*, vol. 29, no. 2, pp. 329–337, Apr. 2002, doi: 10.1139/l02-010.

42. D. Souza, D. Jesus, L. Sanchez, and A. Biparva, "The Use of Self-Healing Technology to Mitigate the Alkali–Silica Reaction Distress in Concrete," in *Proceedings of the Canadian Society of Civil Engineering Annual Conference 2022*, vol. 359, R. Gupta, M. Sun, S. Brzev, M. S. Alam, K. T. W. Ng, J. Li, A. El Damatty, and C. Lim, Eds., in Lecture Notes in Civil Engineering, vol. 359. , Cham: Springer Nature Switzerland, 2024, pp. 1183–1200. doi: 10.1007/978-3-031-34027-7_79.

43. D. Giannantonio, J. Kurth, K. Kurtis, and P. Sobecky, "Molecular characterizations of microbial communities fouling painted and unpainted concrete structures," *Int. Biodeterior. Biodegrad.*, vol. 63, pp. 30–40, Jan. 2009, doi: 10.1016/j.ibiod.2008.06.004.

44. B. Fournier, M.-A. Bérubé, and K. J. Folliard, "Report on the Diagnosis, Prognosis, and Mitigation of Alkali-Silica Reaction (ASR) in Transportation Structures," FHWA Office of Pavement and Technology, The Transtec Group, Final Report FHWA-HIF-09-004, 2010.

45. American Association of State Highway and Transportation Officials (AASHTO), *Manual for bridge element inspection (2nd edition)*, 2nd ed. Washington, DC: American Association of State Highway and Transportation Officials, 2019.

46. M. D. A. Thomas, B. Fournier, K. J. Folliard, and Y. Resendez, "Alkali-Silica Reactivity Surveying and Tracking Guidelines," FHWA Office of Pavement and Technology, The Transtec Group, Final Report FHWA-HIF-12-046, 2012.

47. M. T. Ley and M. Khanzadeh Moradllo, "Expected Life of Silane Water Repellant Treatments on Bridge Decks," Oklahoma Department of Transportation, Oklahoma City, OK, FHWA-OK-15-05, 2015.

48. S. H. Diab, A. M. Soliman, and M. R. Nokken, "Feasibility of basalt and glass FRP mesh for strengthening and confinement concrete damage due to ASR-expansion," *Constr. Build. Mater.*, vol. 266, p. 120893, Jan. 2021, doi: 10.1016/j.conbuildmat.2020.120893.

49. C. Merz and A. Leemann, "Assessment of the residual expansion potential of concrete from structures damaged by AAR," *Cem. Concr. Res.*, vol. 52, pp. 182–189, Oct. 2013, doi: 10.1016/j.cemconres.2013.07.001.

50. M. Ramsey, S. Wood, and R. Moser, "Residual expansion capacity and degradation of mechanical properties in alkali-silica reaction (ASR) damaged concrete," Engineer Research and Development Center (U.S.), Apr. 2019. doi: 10.21079/11681/32485.

51. K. Scrivener, R. Snellings, and B. Lothenbach, *A practical guide to microstructural analysis of cementitious materials*. Crc Press, 2018.

52. C. Szeto and K. E. Kurtis, “Sulphate resistance of low-clinker engineered cementitious composites examined by MicroXRF imaging,” *J. Microsc.*, vol. 294, no. 2, pp. 239–250, May 2024, doi: 10.1111/jmi.13303.

53. D. Kumar, C. Trottier, L. K. Stewart, L. Sanchez, and K. E. Kurtis, “Combined DRI and µXRF for quantitative characterization of damage in ASR-affected concrete: A proof-of-concept investigation,” in *Proceedings of the 17th International Conference on Alkali-Aggregate Reaction in Concrete*, Springer, 2024.

54. American Association of State and Highway Transportation Officials, “AASHTO T 379-18 (2022)Standard Method of Test for Nonlinear Impact Resonance Acoustic Spectroscopy (NIRAS) for Concrete Specimens with Damage from the Alkali–Silica Reaction (ASR).” Washington, DC, 2022.

55. J.-Y. Kim, A. Bellotti, P. Alapati, K. E. Kurtis, J. Qu, and L. J. Jacobs, “Use of a non-collinear wave mixing technique to image internal microscale damage in concrete,” *J. Appl. Phys.*, vol. 131, no. 14, p. 145102, Apr. 2022, doi: 10.1063/5.0086194.

56. F. J. Weiss, J.-Y. Kim, K. E. Kurtis, D. VanderLaan, C. N. Tenorio, and L. J. Jacobs, “Experimental study on the nonlinear mixing of ultrasonic waves in concrete using an array technique,” *NDT E Int.*, vol. 143, p. 103054, Apr. 2024, doi: 10.1016/j.ndteint.2024.103054.